


---

This is the **accepted version** of the journal article:

Azzarà, Beatrice; Cherin, Marco; Iurino, Dawid A.; [et al.]. «An articulated skeleton of *Eucyon monticinensis* (Carnivora: Canidae) from the latest Miocene of Verduno (Italy)». *Zoological Journal of the Linnean Society*, Vol. 203, Issue 4 (April 2025), art. zlaf016. DOI 10.1093/zoolinnean/zlaf016

---

This version is available at <https://ddd.uab.cat/record/310827>

under the terms of the  <sup>IN</sup>  
COPYRIGHT license

**An articulated skeleton of *Eucyon monticinensis* (Carnivora: Canidae) from the latest Miocene of Verduno (Italy)**

Beatrice Azzarà<sup>1,\*</sup>, Marco Cherin<sup>1</sup>, Dawid A. Iurino<sup>2</sup>, Simone Colombero<sup>3</sup>, Daniele Panetta<sup>4</sup>, Marco Pavia<sup>3</sup>, Raffaele Sardella<sup>5</sup>, Leonardo Sorbelli<sup>6</sup>, Lars Werdelin<sup>7</sup>, Giorgio Carnevale<sup>3</sup>

<sup>1</sup>Department of Physics and Geology, University of Perugia, Perugia, Italy

<sup>2</sup>Department of Earth Sciences “Ardito Desio”, University of Milan, Milan, Italy

<sup>3</sup>Department of Earth Sciences, University of Torino, Italy

<sup>4</sup>CNR National Research Council of Italy, Institute of Clinical Physiology, Pisa, Italy

<sup>5</sup>Department of Earth Sciences, Sapienza University of Rome, Rome, Italy

<sup>6</sup>Institut Català de Paleontologia Miquel Crusafont, Universitat Autònoma de Barcelona, c/Columnes s/n, Campus de la UAB, Barcelona, Spain;

<sup>7</sup>Department of Palaeobiology, Swedish Museum of Natural History, Stockholm, Sweden

\* Corresponding author. Department of Physics and Geology, University of Perugia, Perugia, Italy. E-mail: [beatrice.azzara@unipg.it](mailto:beatrice.azzara@unipg.it)

**ABSTRACT**

The genus *Eucyon* includes several Late Miocene–Early Pleistocene canid species, the earliest of which, *Eucyon davisi*, is regarded as basal in the radiation of the Canini. *Eucyon monticinensis* is known from Italy (Late Miocene) and Spain (Early Pliocene). Here we report on an articulated skeleton from Verduno (Italy) referred to *E.*

*monticinensis* based on comprehensive comparisons. The Verduno skeleton stands out as the most complete specimen of *Eucyon* from Europe, and as one of the most complete in the world. The fossil has allowed us to investigate and reconstruct in detail the morphology of *E. monticinensis*. Based on morphological similarity, *Eucyon debonisi* is regarded as a junior synonym of *E. monticinensis*. Computed tomography-based analysis provides some interesting insights into the comparative anatomy of the brain and frontal sinuses of *Eucyon* and other canids. We further present a revised phylogeny of the Canidae based on morphological characters. *Eucyon davis* is confirmed as the most basal species in a monophyletic clade that also includes *E. monticinensis*, *Eucyon zhoui*, and *Eucyon adoxus*. *Eucyon khoikhoi* from South Africa and *Eucyon ferox* from North America show phylogenetic relationships and morphological affinities with the Vulpini and crown-Canini, respectively, which raises questions regarding their systematic status.

**Keywords:** Canini; canid; fossil; Messinian; palaeontology; phylogenetics

## INTRODUCTION

The extinct canid genus *Eucyon* Tedford and Qiu, 1996 (from Greek *eu*, primitive and *cyon*, dog) is recognized as the earliest member of the tribe Canini (Rook 2009), thus playing a crucial role in the understanding of the divergence between this clade and fox-like canids, the Vulpini (Tedford *et al.* 2009). Despite sharing some characters with the genera *Canis* Linnaeus, 1758 and *Lupulella* Hilzheimer, 1906, *Eucyon* lacks some of their apomorphies, such as the transverse crest connecting hypoconid and entoconid in the lower carnassial talonid (Tedford and Qiu 1996, Rook 2009).

The first occurrence of *Eucyon* can be traced back to the Late Clarendonian (Late Miocene; *c.* 10–9 Mya) in North America, specifically in Nebraska, with the presence of *Eucyon davis* (Merriam 1911). In that period, open grasslands were extensively widespread in North America (Wang *et al.* 2008, Tedford *et al.* 2009). *Eucyon davis* persisted in North America until the Late Hemphillian (Early Pliocene), chronologically overlapping for almost a million years with the hypercarnivore *Eucyon ferox* (Miller and Carranza-Castañeda, 1998) (Bartolini-Lucenti and Rook 2021). *Eucyon* dispersed into Eurasia through the Beringian land bridge about 8.0 Mya, with *E. davis* being the only

species recognized both in the Nearctic and the Palaearctic (Tedford and Qiu 1996). In the Late Miocene, *Eucyon* was widely distributed across the Old World, where some species survived until the Early Pleistocene (Perini *et al.* 2010, Sotnikova and Rook 2010). Figure 1 shows the geographical and chronological distribution of all the known species of *Eucyon*. The earliest record in the Old World at *c.* 7.5. Mya is that of *Eucyon cipio* (Crusafont Pairó 1950) in Spain (Pons-Moyà and Crusafont 1978). The presence of *Eucyon* has been documented in numerous Late Miocene to earliest Pleistocene localities, with the following species: *Eucyon davisii*, *Eucyon zhoui* Tedford and Qiu, 1996, *Eucyon* sp. from Kvabebi, ‘*Eucyon*’ *kuruksaensis* (Sotnikova, 1989), *Eucyon marinae* Spassov and Rook, 2006, and *Eucyon minor* (Teilhard de Chardin and Piveteau, 1930) in Asia (Tedford and Qiu 1996, Spassov and Rook 2006, Rook 2009, Sotnikova and Rook 2010, Rook *et al.* 2017); *Eucyon cipio* (Crusafont Pairó 1950), *Eucyon monticinensis* (Rook 1992), *Eucyon adoxus* (Martin 1973), *Eucyon debonisi* Montoya *et al.*, 2009, *Eucyon odessanus* (Odintzov 1967), and *Eucyon* sp. from Mill-Langenboom in Europe (Rook 1992, Kostopoulos and Sen 1999, Radulescu *et al.* 2003, Sardella 2008, Montoya *et al.* 2009, Colombero *et al.* 2014, Peters *et al.* 2015, Piñero *et al.* 2017, Koufos *et al.* 2022); *Eucyon kuta* Werdelin *et al.*, 2015, ‘*Eucyon*’ *intrepidus* Morales *et al.*, 2005, ‘*Eucyon*’ *wokari* García, 2008, and *Eucyon khoikhoi* Valenciano *et al.*, 2022 in Africa (Morales *et al.* 2005, Howell and García 2007, García 2008, Werdelin *et al.* 2015, Valenciano *et al.* 2022). A detailed account of the spatio-temporal distribution and morphology of all these species is presented in Supporting Information, Appendix S1 arranged by geographical areas, and Supporting Information, Table S1 arranged by species.

Amongst all the records of *Eucyon* mentioned above, very few include complete cranial remains (see examples in Fig. 1) and even fewer include articulated skeletons or skeletal parts (in this context, the exceptional skeleton of *E. davisii* F:AM 63010 from Bird Bone Quarry, Arizona stands out; Tedford *et al.* 2009: fig. 39). In this study we report on a well-preserved articulated partial skeleton of *Eucyon* from the late Messinian of Verduno (Piedmont, Italy), representing the most complete specimen of this genus in Europe to date. The fossil offers an invaluable opportunity to investigate the morphology and body proportions of these extinct canids (including some details of their endocranial structures) and also serves as a basis for an updated phylogenetic study.

### **The Verduno palaeontological site within the Messinian palaeogeographical context**

The pre-Messinian Late Miocene land mammal sites of Italy provide compelling evidence for the existence of three distinct palaeobioprovinces: Abruzzo-Apulia, Tusco-Sardinia, and Calabria-Sicily. The vertebrate faunas of Abruzzo-Apulia and Tusco-Sardinia were characterized by strong endemism, thus attesting to the occurrence of isolated emerged areas (Torre *et al.* 2000, Rook *et al.* 2006). The Abruzzi-Apulian palaeobioprovince developed on an archipelago that persisted on the Apulian platform until the Early Pliocene (Patacca *et al.* 2013). This region was characterized by the occurrence of typical endemic elements, such as *Microtia*, which is indicative of long-term geographic isolation (Abbazzi *et al.* 1996, Rook *et al.* 2006).

The Tusco-Sardinian palaeobioprovince, located on the peri-Tyrrhenian side of Italy (southern Tuscany and Sardinia), hosted Late Miocene faunal assemblages referred to an endemic faunal complex known as the ‘*Oreopithecus* Zone Faunas (OZF)’ (Bernor *et al.* 2001) comprising the hominoid primate *Oreopithecus* Gervais, 1872, the antelope *Myaemmmia* Hürzeler 1983, and the giraffid *Umbrotherium* Hürzeler and Engesser, 1976 (Abbazzi *et al.* 2008, Pandolfi and Rook 2023). A few endemic carnivores referable to the subfamily Lutrinae occur in Tuscany, such as *Tyrrhenolutra helbingi* Hürzeler, 1987 (Baccinello V1), *Paludolutra maremmana* Hürzeler, 1987, and *Paludolutra campanii* (Meneghini, 1862) (Monte Bamboli; Ginsburg 1999, but see Faggi *et al.* 2024 for a revised stratigraphy) and the ursid *Indarctos laurillardii* (Meneghini, 1862) (= *Indarctos anthracitis* Weithofer, 1888) (Sardella 2008).

During the Messinian, a dramatic reorganization of the palaeobiogeography of the Apennine chain occurred, leading to changes in terrestrial ecosystems along the entire peninsula. All the taxa belonging to the OZF faunal complex disappeared and were replaced by a new faunal assemblage (Baccinello V3), including continental taxa with clear European affinities (Hürzeler and Engesser 1976, Rook 1999, Rook *et al.* 1999, Abbazzi 2001, Benvenuti *et al.* 2001, Bernor *et al.* 2001). The V3 assemblage, characterized by non-endemic taxa, underscores a definitive palaeobiogeographical connection with Europe. This faunal turnover coincided with the documentation of roughly coeval faunas penetrating into the northern Apennines throughout Piedmont and Romagna, as evidenced by sites such as Ciabòt Cagna, Moncucco Torinese, and Verduno (Piedmont; Cavallo *et al.* 1993, Colombero *et al.* 2014, 2017a), Brisighella (Emilia Romagna; De Giuli *et al.* 1988, Sami 2007, Rook 2021, Villa *et al.* 2022), and several

sites in Tuscany (Fine valley, Casino, Velona, and Baccinello V3; Kotsakis *et al.* 1997, Rook *et al.* 1999, Benvenuti *et al.* 2001).

Additionally, Late Miocene mammals are also reported from sites in southern Italy such as Cessaniti (Vibo Valentia, Calabria; Ferretti *et al.* 2003, Marra *et al.* 2011) and Gravitelli (Messina, Sicily; Seguenza 1902, 1907). Taxa from these sites (e.g. *Stegotetrabelodon syrticus* Petrocchi, 1941 from Cessaniti; Ferretti *et al.* 2003) exhibit clear affinities with those recorded in approximately coeval North African localities (e.g. Sahabi, Libya), suggesting that the Calabria-Sicily area served as a northern extension of the Late Miocene Mediterranean border of the African plate (Rook *et al.* 2006, Marra *et al.* 2011, Pandolfi *et al.* 2021). Regarding the Gravitelli fauna—which included a rhino, several forms of bovids, a hexaprotodont hippopotamid, a colobine monkey, and a suid referable to the genus *Propotamochoerus* Pilgrim, 1925 (Rook 1999, Gallai and Rook 2006, Iannucci 2024)—there is evidence suggesting at least a partial European affinity. Recently, Iannucci (2024) pointed out that the Gravitelli fauna either dates to the late Tortonian or, at most, to the earliest pre-evaporitic Messinian, corresponding to MN11 or MN12 in terms of mammal biochronology. Unfortunately, the fossils from Gravitelli were destroyed during the Messina earthquake in 1908, leaving descriptions by Seguenza (1902, 1907) as the only available source of information on this fauna.

In this paper, we focus on the aforementioned Messinian site of Verduno, located on the left bank of the Tanaro River, in the southern part of the Tertiary Piedmont Basin near the town of Alba, (northern Italy). In the Tertiary Piedmont Basin, the Messinian succession starts with the Myarne di Sant’Agata Fossili Formation, a unit that exhibits a precession-related cyclic stacking pattern characterized by alternating shale and marl couplets (Dela Pierre *et al.* 2011) and locally by diatomites (Carnevale *et al.* 2019, Pellegrino *et al.* 2020a, b). The muddy sediments of the Myarne di Sant’Agata Fossili are followed by the evaporites of the Primary Lower Gypsum unit, which was deposited during the first stage of the Messinian salinity crisis, being formed of gypsum–shale couplets. The Primary Lower Gypsum unit is covered by the resedimented evaporites of the Valle Versa Chaotic Complex that pertains to the second stage of the Messinian salinity crisis (Dela Pierre *et al.* 2007). The upper part of the succession comprises the Conglomerati di Cassano Spinola Formation, a thick unit of fluvio-deltaic and lacustrine deposits (Ghibaudo *et al.* 1985) recording the third stage of the Messinian salinity crisis. In the Verduno site the Conglomerati di Cassano Spinola Formation can be split into two

subunits, of which the lower one consists of fine-grained sediments interpreted as alluvial plain, overbank, or waning flood deposits (Colombero *et al.* 2014). A diverse fossil vertebrate assemblage, comprising cyprinodontiform fishes, amphibians (bufonids and ranids), reptiles (testudinids, geoemydids, lacertids, anguids, varanids, agamids, amphisbaenians, scolecophidians, and colubrids), birds (galliforms, accipitriforms, and strigiforms), and mammals (gomphotheriids, rhinocerotids, equids, cervids, palaeomerycids, camelids, giraffids, bovids, mustelids, canids, felids, hyaenids, ochotonids, cricetids, hystricids, murids, glirids, soricids, and erinaceids), indicative of an open, semi-arid woodland savanna with sparse waterbodies, was recovered from the sediments of this subunit (Colombero *et al.* 2013, 2014, 2015, 2017b) (coordinates: 44° 41' 9" N, 7° 55' 53" E). According to Colombero *et al.* (2014, 2017b), the vertebrate-bearing deposits indicate a late Turolian age and date back to the lower part of the third stage of the Messinian salinity crisis, approximately between 5.55 and 5.40 Mya.

### **Abbreviations**

BRS, Brisighella collection hosted at the Department of Earth Sciences of the University of Florence, Italy; F:AM, Frick Collection, Division of Paleontology, American Museum of Natural History (AMNH), New York, USA; GIN, Geological Institute, Russian Academy of Science, Moscow, Russia; IPS, Institut Català de Paleontologia Miquel Crusafont, Barcelona (ICP), Spain; IVPP, Institute of Vertebrate Paleontology and Paleoanthropology, Beijing, China; MAB, Oertijdmuseum De Groene Poort, Boxtel, The Netherlands; MC, Museo Civico di Zoologia di Roma, Italy; MCEA, Museo Civico 'Federico Eusebio' of Alba, Italy; MFS, Museo Civico di Scienze Naturali, Faenza, Italy; MGPT-PU, Museum of Geology and Paleontology, University of Turin, Italy; MGUV, Museu de Geologia de la Universitat de València, Burjassot, Spain; MNCN, Museo Nacional de Ciencias Naturales, Madrid, Spain; NMB, Naturhistorisches Museum Basel, Switzerland; NME, National Museum of Ethiopia, Addis Ababa, Ethiopia; NRM, Swedish Museum of Natural History, Stockholm, Sweden; MSNG, Natural History Museum of Genoa; PIN, Palaeontological Institute, Russian Academy of Science, Moscow, Russia; SAM-PQL, Cenozoic Palaeontology collection, Iziko South African Museum, Cape Town, South Africa; SAM-ZM, Terrestrial Vertebrates collection, Iziko South African Museum, Cape Town, South Africa; UCMP, Museum of Paleontology, University of California Berkeley, USA; UO, University of Oregon, Museum of Natural History, USA.

## MATERIALS AND METHODS

### Fossil material and comparative samples

The canid skeleton analysed in this work is part of the Upper Messinian vertebrate assemblage collected at Verduno (Piedmont, north-western Italy) by the palaeontology team of the Department of Earth Sciences, University of Turin. Following the code used by the research group, the specimen has been labelled as MGPT-PU 135418.

The Verduno specimen was compared with the following Late Miocene to Early Pleistocene *Eucyon* specimens (Fig. 1): *E. davis* (UCMP 545, UCMP 112197, UO 12505, UO 12543, F:AM 63007, F:AM 63008, F:AM 63009, F:AM 63009B, F:AM 63038, F:AM 63058) and *E. ferox* (F:AM 72556, F:AM 72566, F:AM 72569A) from North America; *E. davis* (F:AM 97028, F:AM 97056, F:AM 97057, F:AM 97059, F:AM 97061) and *E. zhoui* (F:AM 97048) from China; *E. cipio* from Concud (IPS 1988) and Los Myansuetos (IPS 46489); *E. monticinensis* from Brisighella [MSF 94 (BRS 27/4), MSF 98 (BRS 27/15), MSF 99 (BRS 27/14), MSF 100 (BRS 27/16), MSF 101 (BRS 27/13), MSF 456 (BRS 27/47), MSF 457/1, MSF 458 (BRS 27/6), MSF 459, MSF 460, MSF 461 (BRS 27/7), MSF 462 (BRS 27/10), MSF 463, MSF 466, BRS 5/292, BRS 24/12, BRS 27/5, BRS 27/21, BRS 27/24, BRS 27/27, BRS 27/45, BRS 27/46] and from Verduno (MCEA P01080, MCEA P00991); *E. adoxus* (NMB Rss.45) from Perpignan; *E. odessanus* (PIN 390- 156, PIN 390-160) from Odessa. Further comparative data were taken from the literature, including Merriam (1911), Teilhard de Chardin and Piveteau (1930), Odintzov (1967), Martin (1973), Pons-Moyà and Crusafont (1978), Rook (1992, 1993), Tedford and Qiu (1996), Kostopoulos and Sen (1999), Morales *et al.* (2005), Spassov and Rook (2006), Garcia (2008), Sardella (2008), Haile-Selassie and Howell (2012), Lyras (2009), Montoya *et al.* (2009), Rook (2009), Sotnikova and Rook (2010), Ivanoff *et al.* (2014), Sardella *et al.* (2014), Peters *et al.* (2015), Werdelin *et al.* (2015), Piñero *et al.* (2017), Rook *et al.* (2017), Basili *et al.* (2018), Bartolini-Lucenti and Rook (2021), Koufos (2022), Valenciano *et al.* (2022), Bartolini-Lucenti *et al.* (2022), Iurino *et al.* (2022a, b), Frosali *et al.* (2023).

Craniodental and postcranial measurements were taken with digital callipers to the nearest 0.1 mm following Von den Driesch (1976) and Valenciano *et al.* (2021). The upper teeth are indicated with uppercase letters, the lower teeth with lowercase letters.

To compare the dental proportions between *Eucyon* species from North America, Eurasia, and Africa, we used log10 ratio diagrams (Simpson 1941, Simpson *et al.* 1960). The extant *Canis aureus* (Linnaeus 1758) was selected as the reference baseline in these diagrams due to the *Eucyon*-like overall size and the abundance of available biometric data ( $N = 70$ ; measurements collected at NRM and MSNG and by bibliographic sources, but only in cases of certain taxonomic attribution and/ or precise geographical origin of the samples). The variables used in log10 ratio diagrams were the length and width of P1– M2 and of p2–m2.

The body mass of the *Eucyon* individual from Verduno and the average for all known *Eucyon* species were calculated using the prediction equation by Van Valkenburgh (1990) on the basis of the length of the lower carnassial.

### **Virtual palaeontology**

A series of different techniques was used to obtain 3D models of the specimen MGPT-PU 135418. *Structure-from-Motion* photogrammetry was applied to build 3D models before (Fig. 2) and during the extraction from the matrix of the skeleton and its preparation, carried out at the Department of Physics and Geology, University of Perugia. Photographs were taken with a Canon EOS 500D DSLR camera with 18–55 mm lens used at 35 mm for the 3D model of the whole block before preparation, and with a Nikon D750 DSLR camera with 28–75 mm lens used at 50 mm for the 3D models of portions of the skeleton as they were extracted from the block. All the photos were taken freehand and with natural light. The 3D models were built and scaled using software Agisoft PhotoScan Pro v.1.3 (Agisoft 2014).

The forelimb bones (except for the scapulae), 5th and 6th thoracic vertebrae, rib fragments, and sternum were all extracted from the block. 3D models of all these skeletal elements were built with a structured-light 3D scanner Artec Space Spider (resolution: 0.1 mm). Each bone was placed on a turntable, with the scanner held by the user. The turntable was then rotated slowly, while the scanner was held still or moved slightly to capture the entire surface of the specimen. The scans were made at 7–8 frames per second. Data were processed using software Artec Studio v.15 (Artec 3D). After alignment, any meshes with errors higher than 0.3 mm were deleted from the batch.

A smaller block containing the 2nd to 7th cervical vertebrae, 1st to 4th thoracic vertebrae, and the scapulae was left unprepared so as not to jeopardize the integrity of the

bones. This block and the skull were scanned with a micro-CT industrial device at Microservice s.r.l. (Alpignano, Turin). Technical settings are reported in Supporting Information, Table S2. Tomographic images of *Canis lupus lycaon* Schreber, 1775, *Canis lupus baileyi* Nelson and Goldman, 1929, and *Canis simensis* Rüppell, 1840 were downloaded from MorphoSource.org (ark:/87602/m4/M113796, ark:/87602/m4/M114099, ark:/87602/m4/M113802); those of *Canis etruscus* Forsyth Major, 1877 and *Canis arnensis* Del Campana, 1913, were taken using a Philips Brilliance CT 64-channel scanner at Azienda Ospedaliero-Universitaria Careggi (Florence, Italy); those of the rest of the sample (complete list in Supporting Information, Table S3) were taken using a Philips Brilliance CT 64-channel scanner at M.G. Vannini Hospital (Rome, Italy). All the specimens were scanned from front to back in the coronal slice plane. The slice thickness is 0.67 mm with an interslice space of 0.33 mm. The brain endocast of *Eucyon davisi* F:AM 97057 was obtained by high-resolution computed tomography (500 slices) at the University of Texas X-ray CT facility (Lyras 2009). Tomographic images were processed and analysed using software MIMICS 21.0 (Iurino *et al.* 2013) and 3D Slicer 4.11 (Fedorov *et al.* 2012). Segmentations were then exported to meshes in STL format, then optimized in MeshLab v.2021.05 (Cignoni *et al.* 2008). Software CloudCompare 2.12 (Girardeau-Montaut 2020) and MIMICS 21.0 (Materialise®) were used to visualize and analyse (i.e. measure) the 3D models. The final rendering of the 3D models and the process of bone alignment to obtain a virtually articulated skeleton were carried out with ZBrush 4R6 (Papstein *et al.* 2015).

### Phylogenetic analysis

We performed a maximum parsimony analysis using TNT v.1.6 (Goloboff and Morales 2023) based on a matrix (Supporting Information, Appendix S2) including 19 taxa and 76 characters (33 of the cranium, four of the mandibles, 37 of the teeth, and two of postcranial bones) based on Tedford *et al.* (2009), Prevosti (2010), Zrzavý *et al.* (2018), and this work. *Leptocyon vafer* (Leidy, 1858) was set as the outgroup. Two extant Vulpini, *Vulpes vulpes* Linnaeus, 1758 and *Nyctereutes procyonoides* Gray, 1834, were scored. Among *Eucyon* species, we included in the analysis only those with sufficiently complete and well-preserved cranial material, namely *E. davisi*, *E. zhoui*, *E. adoxus*, *E. ferox*, *E. khoikhoi*, and the new specimen from Verduno. The extant Canini examined were *Lupulella mesomelas* (Schreber, 1775), *Lupulella adusta* (Sundevall, 1847), *Canis lupaster* Hemprich and Ehrenberg, 1832, *Canis aureus* Linnaeus, 1758, *Canis latrans*

Say, 1823, *Canis lupus* Linnaeus, 1758, and *Lycaon pictus* Temminck (1820), to which we added the extinct species *C. etruscus*, *C. arnensis*, and *Aenocyon dirus* (Leidy, 1858). Characters (Supporting Information, Appendix S2) were weighted equally, multistate characters were left unordered, and the analysis was conducted by ‘New Technology search’ (default settings).

## **RESULTS**

### **Systematic palaeontology**

#### **Order Carnivora Bowdich, 1821**

#### **Suborder Caniformia Kretzoi, 1943**

#### **Family Canidae Batsch, 1788**

#### **Subfamily Caninae Batsch, 1788**

#### **Tribe Canini Batsch, 1788**

#### **Subtribe Canina Batsch, 1788**

#### **Genus *Eucyon* Tedford and Qiu, 1996**

#### ***Eucyon monticinensis* (Rook, 1992)**

**(Figs 3–7)**

- 1991 «*Canis*» sp. Rook *et al.*: 19, Pl. 3
- 1992 «*Canis*» *monticinensis* Rook: 151, fig. 1.
- 1993 *Eucyon monticinensis* Rook: Tav. III, figs 4–6.
- 1993 *Eucyon* cf. *monticinensis* Rook: Tav. III, figs 7–10.
- 2008 *Eucyon monticinensis* Sardella: 200, fig. 5.
- 2009 *Eucyon debonisi* n. sp. Montoya *et al.*: 713–714, figs 1, 2; 716–717, figs 3, 4
- 2014 *Eucyon monticinensis* Colombero *et al.*: 307, fig. 11.3–11.9.
- 2017 *Eucyon monticinensis* Piñero *et al.*: 110, fig. 7.J2–J4.
- 2021 *Eucyon monticinensis* Bartolini-Lucenti *et al.*: 133–149, fig. 7
- 2022 *Eucyon monticinensis* Bartolini-Lucenti *et al.*: 1459, fig. 1.c–f, 1.k–l.

- 2023 *Eucyon monticinensis* Frosali *et al.*: Figs 3B- 3B', 3E-3E'

*Emended diagnosis:* A canid about the size of an extant jackal. The splanchnocranium is short, stout, and tapered, showing a subtle constriction immediately behind the canine alveoli. The neurocranium is elongated. The basioccipital is narrow between the bullae and shows a narrow crest running along the sagittal axis. The postorbital constriction is narrow and has further narrowing in its middle part. The olfactory bulb of the brain is prominent, dorsoventrally expanded, and laterally compressed. The cerebrum lacks the endolateral sulcus. The frontal sinuses are wide with the rostromedial lobe strongly reduced; the rostral incision is missing; the dorsocaudal lobe is large with a rounded margin. The ramus is relatively short; shallower and less robust than that of *Canis* spp.; the angular process is slender with a very slightly expanded inferior pterygoid fossa [Type A in Gaspard (1964: fig. 24)]; the subangular lobe is more expanded than that of *Vulpes* spp. In the M1, the paracone and metacone are subequal in size, the metaconule and protocone are joined by a strong postprotocrista, the parastyle is not very strong, and the buccal cingulum is well developed. The m1 has a distinct metaconid, a large and sturdy protoconid, a relatively well-developed talonid, whose hypoconid and entoconid are not joined by a transverse cristid, and a relatively strong entoconid. The radius/tibia ratio is slightly greater than 80% (modified from: Rook 1992).

*Holotype:* MSF 97 (BRS 27/4), right mandibular ramus with p2 and m1.

*Type locality:* Monticino gypsum quarry (Brisighella, Faenza, Italy), from site BRS 27.

*Chronological distribution:* Latest Miocene to earliest Pliocene (approximately from 5.5 to 4.9 Mya; Colombero *et al.* 2014, Piñero *et al.* 2017), correlative with the Turolian-Ruscinian (i.e. MN 13-14) transition in the European land mammal-based biochronological framework (Ezquerro *et al.* 2022).

*Geographic distribution:* The species is reported in the latest Miocene (5.55–5.33 Mya) of northern Italy (sites of Monticino and Verduno; Rook 1992, 2009, Sardella 2008, Colombero *et al.* 2014) and the earliest Pliocene (4.997–4.896 Mya) of southern Spain (site of Puerto de la Cadena; Piñero *et al.* 2017). In Italy, the species might also occur in the Casino Basin (Tuscany; latest Miocene), but the material is too fragmented for a species-level identification [*Eucyon* sp. in Rook (2009)]. In Spain, the sample from Venta del Moro (latest Miocene) previously referred to *E. monticinensis* (Rook 1992) or *E. cf.*

*monticinensis* (Spassov and Rook 2006), has been subsequently assigned to the similar species *E. debonisi* (Montoya *et al.* 2009) (Fig. 1).

*Referred material:* MGPT-PU 135418, a partially complete articulated skeleton comprising the skull with almost complete dentition (right i1 and p1 and left i1 are missing), all cervical and first four thoracic vertebrae, slightly displaced 5th and 6th thoracic vertebrae, well-preserved right and incomplete left scapulae, right and left humeri, complete left and proximal right radii, complete left and proximal right ulnae, six left carpals, left I–V metacarpals, I–V proximal phalanges, I–IV intermediate phalanges, and III–IV distal phalanges, six sesamoids, fragmented ribs, and sternum. Measurements of the studied specimen are in Tables 1–3.

### *Description*

*Cranium* The cranium (Figs 3A–E, 5) is remarkably well preserved, although it has undergone plastic diagenetic deformation towards the left side. Consequently, the right orbit appears more elongated than the left one. Both the zygomatic arches are broken in their posterior half and the sagittal crest is incomplete. All endocranial cavities are completely filled by rock matrix.

In lateral view, the dorsal outline of the cranium is gently convex, with only a slight concavity in the middle of the muzzle. The left orbit has preserved its original shape, being taller than long, with its primary axis inclined relative to the anteroposterior axis of the cranium. The infraorbital foramina, located above the P3, are faintly visible due to diagenetic obliteration. The neurocranium is relatively elongated, while the splanchnocranium is short and stout with a short premaxilla. A depression is clearly visible at the level of the anterior end of the frontal sinuses, just anterior to the sagittal crest. The nuchal crest is directed dorsally and extends posteriorly well beyond the occipital condyles. The paroccipital process is ventrally directed with a curved posterior margin (i.e. following the shape of the tympanic bulla) showing approximately the same height as the bulla.

In dorsal view, the elongation of the neurocranium is clearly visible. The splanchnocranium is tapered, with a thin constriction immediately posterior to the canine alveoli. Based on what is exposed due to taphonomic obliteration, the posterior margin of the nasal bones seems not to extend beyond the frontomaxillary suture. The internasal and interfrontal sutures reside within a deep sagittal groove, whose depth may be

exaggerated by deformation. The left zygomatic arch is better preserved; it opens anteriorly with a step and displays an almost straight lateral margin. The postorbital processes of the frontals are wide and their anterior and posterior margins form an angle of about 45° with the sagittal axis of the cranium (i.e. the postorbital process has a shape resembling an isosceles triangle). Posteriorly to the postorbital processes, the temporal crests are strong and slightly convex towards the sagittal axis. These crests merge posteriorly into a short sagittal crest at about midlength of the braincase. This crest connects posteriorly to a prominent and narrow nuchal crest, which is damaged on the right side. The postorbital constriction is narrow with a strongly constricted middle part. The parietal bones are rounded and expanded, so that the maximum width of the neurocranium is greater than the frontal width. The left dorsal surface of the neurocranium is damaged, thereby exposing small portions of a natural endocast.

In ventral view, the basal part of the cranium is not fully visible due to the presence of the mandible, which is displaced towards the left side. The palate (clearly visible in CT scans; Fig. 5J) is fully preserved, but the density of the rock matrix covering the palate has prevented detailed segmentation. Compared to the size of the cranium, the tympanic bullae are relatively small with a leaf-shaped outline and a slight medial compression; the medial walls are convergent anteriorly. Consequently, the basioccipital is narrow between the bullae, and shows a strong narrow crest running along the sagittal axis. The mastoid processes are wide and robust. The occipital condyles are well preserved and extend laterally, reaching nearly to midwidth of the tympanic bullae.

In posterior view, the diagenetic deformation of the neurocranium is easily recognizable. The left part of the braincase appears to be more bulging and more dorsally enlarged than the right one. The occipital squama is bell-shaped, relatively wide, and low. The foramen magnum is dorsoventrally flattened by diagenesis. The right paraoccipital process is better preserved than the left one and is strong and ventrally pointed.

*Brain and frontal sinuses* The brain endocast (Figs 5, 6) consists of a globular telencephalon with prominent and well-preserved olfactory bulbs. Almost the entire caudal region of the cerebellum and the ventral portion of the cerebrum, including the brain stem and cranial nerves, are missing due to the dense infilling matrix which prevented their segmentation. Despite this, the overall brain morphology is clearly recognizable. The total volume is 70 cm<sup>3</sup>, 67 cm<sup>3</sup> without the olfactory bulbs, the telencephalon has a length of 60 mm and a maximum width of 55.6 mm, although this

value is affected by the cast deformation (see Supporting Information, Tables S3, S4). While exhibiting an outline relatively similar to that of *E. davisi* (Lyrras *et al.* 2001, Ivanoff *et al.* 2014), this region is not sufficiently preserved to allow more detailed comparisons.

In dorsal view, the olfactory bulbs are relatively narrow and elongated, characterized by numerous ramifications forming an irregular texture. The telencephalon appears rounded in shape with a slight constriction at the lateral sulcus (sylvian fissure) and a very prominent right temporal lobe resulting from the plastic deformation towards the left side of the cranium. Consequently, the longitudinal fissure divides the cerebrum into two roughly symmetrical hemispheres where the pattern of convolutions is only partially recognisable (Fig. 5). The frontal pole cortex is anteroposteriorly elongated, the orbital gyri are narrow, poorly developed and mostly covered by the prorean gyri. In both hemispheres, the sigmoid and coronal gyri are clear and separated by a marked coronal sulcus (for the complete list of the brain convolutions see Fig. 6).

In lateral view, the olfactory bulbs are strongly developed and projected anteriorly, forming a large spongy pad supported by two robust olfactory peduncles. The dorsal profile of the cortex is rather flat, especially at the frontal pole where the proreous and precruciate gyri converge. This is probably due to the extensive development of the frontal sinuses (Fig. 5). In the rostral region, just before the olfactory bulbs, a short, vertically oriented section of the rhinal sulcus is visible. On the frontoparietal lobes, the convolutions are barely visible and are listed in Fig. 6. The coronal gyrus occupies a very elevated position and partially covers the sigmoid gyrus. The surface of the temporal and occipital lobes is irregular and does not allow for a detailed description of the cerebral convolutions.

The frontal sinuses are large in size and expand caudally, covering a large portion of the endocranial cavity. The rostral lobes extend rostrally, being elongated and rounded, with a small indentation near the posterior part of the eye sockets. The caudal lobes extend slightly towards the frontoparietal sutures, but do not reach them. The ventral lobes extend slightly downward, having a slender and flattened shape. The frontal sinus shows rostralateral lobes that extend forward and are larger compared to the highly reduced rostromedial lobes. In addition, the rostralateral lobe forms a right angle with the postorbital lobe, which extends towards the zygomatic process. Conversely, the lateral dorsocaudal lobes are smaller than the medial one, giving to the frontal sinus a round

shape shifted to the medial dorsocaudal lobe. There are no apparent incisions in the rostral or caudal region. Additionally, both the frontal sinuses exhibit a marked ridge that follows the contour of the prominent sagittal crest.

*Mandible* The mandible is still articulated with the cranium (Fig. 3B, C). The right condyle is still articulated with the glenoid cavity, while the left one is slightly shifted ventrally. In lateral view, the corpus is slender, anteriorly tapering, with a curved posteroventral margin. The coronoid process is very high and tapering. The deep masseteric fossa has a well-outlined anterior margin and is delimited by a distinct masseteric crest. The latter rises dorsocaudally showing an angle in the middle. Two mental foramina of subequal size are present: one is placed below the midlength of p1, the second just below the distal root of p3. The angular process is slender and hook-shaped, with a very slightly expanded inferior pterygoid fossa. The fossa for the inferior pterygoid muscle is small but deep.

*Upper dentition* The upper incisors are progressively larger from I1 to I3. The I2 is slightly larger than I1. No distal cingulum is present in either of these teeth. A small distal accessory cusp is present in I2. The I3 is reduced, like the I2, with a weak basal lingual cingulum. The left I3 has a broken crown and was found isolated in the sediment during the preparation of the fossil (Fig. 7A).

The upper canines are very long, slender, and moderately curved. On the mesial side, the tip shows a clear wear facet. The C is separated from the I3 by a long diastema, in which the c fits.

All the upper premolars are separated by diastemata (Figs 5B, 7A). The longest are found between C and P1 and between P1 and P2, being similar in length. The diastema between P2 and P3 follows, followed by the diastema between P3 and P4. The P1 is much smaller than P2 and P3; it possesses a single conical cusp, with subvertical mesial margin and concave distal one in labial view; the occlusal outline is elliptical; the distal cingulum is present. The P2 and P3 are subequal in size and morphology, having an asymmetric triangular shape in labial view, with the principal cusp placed mesially; no distal accessory cusps are present, while the distal cingulum is weak in both teeth. In lateral view, P4 is dominated by a strong, distally-oriented paracone; the protocone is relatively long and moderately slender, oriented distolingually; the metastyle is nearly the same length as the paracone but is lower in height and almost flat. In occlusal view, the

protocone is short, with a sharp tip and mesiolingual orientation; it is connected to the tip of the paracone by a crest; the parastyle is moderately developed.

The M1 shows a triangular outline in occlusal view, with almost straight labial, mesiolingual, and distolingual sides, and the talon oriented distolingually (Fig. 7A). The parastyle is pointed and notably developed. All the principal cusps are in a moderate state of wear. The paracone and metacone are subequal in size. The protocone and metaconule are well developed, subequal in size, and connected by a strong postprotocrista. The paraconule seems to be present. The talon is directed lingually and hosts a strong hypocone. The contact area between M1 and M2 is reduced. With respect to M1, M2 is reduced in size, with a more oval occlusal outline and a markedly curved mesial margin. In contrast to M1, the paracone is slightly larger than the metacone. No parastyle is observed. The protocone is larger than the metaconule and is connected to the former by a weak postprotocrista. In contrast to M1, the paraconule is present and large; the hypocone is quite low.

*Lower dentition* The left and right i1 are not preserved. The right i2-i3 are in the alveoli, while the left ones were found in the rock matrix (Figs 3F, 4L). The i3 is slightly larger than i2. The latter has a straight occlusal margin in labial view, while in i3, this margin slopes distally. The i3 shows a very small distal accessory cuspid and a more distinct, low mesial cuspid.

The right c is still in place but partially covered by matrix, while the left one was found in the sediment (Figs 3G, 4L). It has a relatively robust and gently curving shape. No labial cingulum is present, while the lingual cingulum is weak.

The lower premolars (Fig. 7B) are separated by diastemata of similar relative lengths as those described for the upper premolars. p1 is only preserved on the left side, but the crown is damaged. It is monocuspid, small, and (presumably) sub-conical; no distal cingulum is present. The p2 is slightly smaller than p3; both have a principal cuspid with a straight mesial edge and curved distal edge in labial view. No additional cuspids are visible, while the distal cingulum is weak. The p4 is larger than the other premolars. Two distal accessory cuspids are present: the main cuspid is well developed, while the second is faintly visible. The distal cingulum is present and well developed.

The m1 possesses a distally projected mesial margin and the typical canid structure, including a strong paraconid with a weakly curving mesial margin (Fig. 7B). The

paraconid is relatively slender and adjacent to the protoconid. The metaconid is pointed and relatively large, placed adjacent to the protoconid. No mesoconid or entoconulid can be seen in the CT scans. The talonid is relatively short and shows a well-developed hypoconid at about midlength. No hypoconulid is present. The hypoconid is wide and larger than the entoconid. No transverse cristid is present between the hypoconid and entoconid. The m2 has a trapezoidal outline in occlusal view. The protoconid and metaconid are subequal in size, aligned mesiodistally and connected by a low cristid. Distal to the protoconid, the hypoconid is present and is much larger than the (cristid-like) entoconid. The m3s can only be observed through CT scans, revealing their distinct oval occlusal shape and a single root. Unfortunately, no other features can be distinguished in the CT scans.

*Postcranial skeleton* The preservation of the atlas is inadequate (Fig. 3H). The left wing is missing and the right one is damaged along the lateral margin. In dorsal view, the body is quite elongated. The dorsal arch is relatively flat, also due to the limited development of the dorsal tubercle. The wide intervertebral foramina open in the craniolateral parts of the dorsal surface. Only the left posterior articular surface is preserved, although very damaged. No ventral tubercle is developed on the ventral side of the body.

All the other cervical and the first four thoracic vertebrae are still articulated with each other and embedded in a rock block, which also includes the two scapulae (Fig. 4A1, A2). For this reason, it is possible to describe their morphology mostly thanks to CT scans. Overall, the axis is well preserved, although the cranioventral edge of the spinous process is slightly curved but fragmented posteriorly; the transverse processes are broken. The remaining cervical vertebrae show slight variations from one another. In lateral view, they show progressively shorter bodies from the 3rd to the 7th. The spinous process is broken in the 3rd and 4th vertebrae. The left transverse processes are also missing, while the right ones are better preserved and almost intact in the 6th. In the 7th, the right transverse process is short, stout, and oriented dorsolaterally; the spinous process is incomplete and oriented in the cranial direction. The bodies of the preserved thoracic vertebrae are similar in length, and relatively shorter than that of the 7th cervical. The spinous processes of the 1st–4th thoracic vertebrae are almost complete and progressively shorter; those of the 5th–6th thoracic vertebrae are broken. The transverse processes are well preserved in the first five thoracic vertebrae and are progressively shorter from the

1st to the 6th. Those of the 1st–3rd vertebrae are directed laterally, while those of the 4th–6th vertebrae are directed craniolaterally.

The right scapula is nearly complete, whereas the left one lacks several portions of the articular area, spine, and blade. In lateral view, the spine is slender and straight; the neck is wide but thin. Unfortunately, the acromion is broken, although it seems to be relatively slender. The scapular tuberosity, visible in the craniolateral part of the articular area, is not well developed. In ventral view, the glenoid cavity is shallow and oval.

Both humeri are very well preserved (Fig. 4C1, C2). The left is slightly abraded in the area of the deltoid tuberosity, while the right is more severely damaged along the medial side of the shaft. In cranial view, the lesser trochanter shows a convex proximal margin and is delimited medially by a weak crest and laterally by the strong anconeal crest, which in fact is connected to a lower crest running diagonally all along the shaft until the trochlea. The shaft is gently curved. The teres and deltoid tuberosities are faintly visible on the proximal shaft medial and distal to the greater tubercle, respectively. In the distal epiphysis, the radial fossa is relatively shallow and the supratrochlear foramen is small. The crest-like greater tubercle is stronger, higher, and thinner than the head. The medial epicondyle is much more developed than the lateral one. In posterior view, the medial protrusion of the lesser tubercle is particularly evident. The head is flat. No nutrient or epicondylar foramina are visible. The posterior surface of the shaft is traversed by a longitudinal crest that joins the lateral epicondyloid crest distally. The latter is particularly strong in its distal part. The olecranon fossa is very deep, being delimited medially by a very strong crest-like caudal process of the medial epicondyle. The curvature of the shaft is clearly exposed in this view. In lateral view, the head is oval, being elongated along the sagittal plane. The greater tubercle is relatively low, being only slightly higher than the head; it shows a distinct pointed process on its posterior extremity, just before the notch with the head. The neck is relatively wide. The proximal part of the diaphysis is traversed longitudinally by the strong anconeal crest, which runs distally until about one third of the shaft length. The shaft has an overall sigmoid development. In medial view, the lesser tubercle stands out as particularly protruding. The intertubercular groove is wide and deep. The third trochanter is strong and curved, following the shape of the shaft. In proximal view, the greater tubercle is straight and directed medially. In distal view, the larger size of the medial epicondyle with respect to the lateral one is particularly evident.

The left radius is complete, whereas only the proximal epiphysis and a fragment of the proximal shaft of the right radius are preserved (Fig. 4D1, D2). In proximal view, the articular surface is oval and divided into two regions, a deep and wide medial one, and a smaller lateral one. A well-defined pointed process is visible at the craniomedial corner of the articular area. This process is clearly visible in cranial view and forms a distinct step with the medial wall of the shaft. The shaft has sub-parallel lateral and medial edges and is overall slightly curved distolaterally. The radius widens dramatically in the mediolateral direction at the distal epiphysis, which is massive. The latter is delimited medially and laterally by very shallow longitudinal grooves (one for the tendon of the abductor pollicis longus muscle and the other for the tendon of the extensor carpi radialis muscle). Conversely, the groove for the tendon of the extensor digitorum communis, located in the craniolateral part of the distal epiphysis, is much deeper. In posterior view, the interosseous crest starts at about midlength and midwidth of the shaft and runs obliquely towards the lateral edge of the distal epiphysis. In lateral and medial views, the radius shows a marked cranial convexity. In distal view, the carpal articular surface has an eye-like outline, being elongated and pointed towards the lateral and medial edges, and more rounded along the cranial and posterior ones.

The left ulna is complete, whereas the right one is preserved only in its proximal part (Fig. 4E1, E2). In cranial view, the proximal portion shows a double twist, with the olecranon area facing craniomedially and the proximal part of the shaft facing craniolaterally. As a result, the humeral articulation is inclined in a proximomedial to distolateral direction. The olecranon is quite short, elongated cranially, and grooved posteriorly. In cranial view, the shaft appears almost straight, with only a slight sigmoid curvature. It is longitudinally traversed by a prominent interosseous crest, which becomes particularly strong in the distal portion. In lateral view, the anconeal process is prominent and is more expanded cranially than the medial projection of the coronoid process, which delimits the trochlear notch distally. The lateral projection of the coronoid process is much less developed than the medial one. The two form the proximal edge of the shallow radial notch, which has a triangular shape pointing distally. A deep longitudinal fossa develops posterior to the lateral projection of the coronoid process at about midwidth the medial surface of the olecranon. A marked crest runs from the distal edge of the medial projection of the coronoid process along most of the mid-longitudinal axis of the shaft. The styloid process at the distal end of the ulna, is slightly oriented medially.

Six out of seven carpal bones of the left side are preserved (Fig. 4F). The scaphoid lacks the medial half: its proximal surface is markedly convex, while on the distal surface, only two concave facets, for the articulation of the trapezoid and capitate, are preserved. The cuneiform is almost flat, while the pisiform has a posteriorly elongated shape with an enlarged and hemispherical posterior head. The trapezoid is small and wedge-shaped, with a slightly convex proximal surface and a convex distal one. The capitate is of about the same size of the trapezoid, but with a cranial surface of the opposite shape, i.e. tapering medially rather than laterally; its posterior portion is broken. The unciform has a trapezoidal and convex distal surface and shows a posterior enlargement.

All the left metacarpals are preserved. Metacarpal I lacks the lateral part of the proximal epiphysis. Metacarpal II is damaged in both the proximal and distal extremities. Its proximal surface is sub-triangular in proximal view, with the cranial and lateral sides forming a right angle. Metacarpals III and IV are long and straight; in the former, the proximal articular surface is trapezoidal, while it is sub-rectangular in the latter. Metacarpal V is laterally enlarged, especially in the proximal and distal ends; in proximal view, the proximal articulation shows a medial half-moon shaped convex surface and a laterally protruding stout process.

All left phalanges are preserved with the exception of distal phalanges I and II. The intermediate and distal phalanges V are still articulated. Six sesamoid bones are also present.

## DISCUSSION

*Eucyon* is a relatively common member of the Late Miocene and Pliocene carnivore guilds in North America, Eurasia, and, somewhat later, in Africa as well, while in the first part of the Early Pleistocene its presence seems limited to some areas of Asia (Fig. 1). With a few exceptions, most of the records consist of dentognathic remains. Complete skulls of *Eucyon* are quite rare, and some of the available specimens have undergone partial reconstruction (Fig. 8).

The specimen from Verduno described above represents the most complete skeleton of *Eucyon* from Eurasia. While the discovery at Verduno presents a unique opportunity to enhance our understanding of the anatomy of this canid, the lack of sufficiently complete comparative specimens is challenging.

## Morphological comparisons

Due to the vast amount of data, the main craniodental morphological differences and similarities between the Verduno fossil and the different species of *Eucyon* are detailed in Supporting Information, Table S5. Given the limited availability of postcranial material confidently referred to *Eucyon*, some comparative information is provided here.

The atlas of *E. khoikhoi* closely resembles that of MGPT-PU 135418. The sole distinction can be seen in posterior view, where the dorsal arch of MGPT-PU 135418 features a prominent triangular dorsal tubercle positioned centrally, which is absent in *E. khoikhoi*. Likewise, the axis of *E. khoikhoi* (SAM-PQL-31272 and SAM-PQL-15174) has remarkable similarity to that of MGPT-PU 135418. The only difference is that in lateral view, the axis of *E. khoikhoi* displays a more linear cranioventral edge of the spinous process, which is more curved in MGPT-PU 135418. No significant differences were detected between the other homologous vertebrae of the two samples.

Regrettably, only the distal portion of the scapula of *E. khoikhoi* (SAM-PQL-40041) is known. Nevertheless, it seems that the neck of the scapula is notably slenderer than that of MGPT-PU 135418.

The general morphology of the humerus and radius-ulna of *E. ferox* and *E. khoikhoi* are similar to those of MGPT-PU 135418, albeit with some notable differences, illustrated below. On the other hand, *E. monticinensis* shows an almost identical morphology. In proximal view, the humerus of *E. ferox* displays a wider and more distally directed head, whereas that of *E. khoikhoi* features a notably smaller head than MGPT-PU 135418; the greater tubercle in *E. ferox* is directed more laterally and the distance between the greater tubercle and the head is shorter (in *E. khoikhoi* the greater tubercle is broken). In cranial view, the humerus of both species has a straighter and slenderer shaft, a strong and straight third trochanter, a broader and more robust anconeal crest, and a more prominent lateral epicondylar crest. In *E. ferox*, the medial epicondyle is more pointed, giving the distal area a triangular shape, while in *E. khoikhoi*, the medial epicondyle is less pointed and lower (similar to *E. monticinensis* and MGPT-PU 135418). Additionally, in *E. ferox*, the trochlea converges slightly into the olecranon fossa, while in *E. khoikhoi*, it is slightly inclined laterally. The trochlea is straight both in *E. monticinensis* and MGPT-PU 135418.

In both *E. ferox* and *E. khoikhoi*, the radius has a straighter and stouter shaft than MGPT-PU 135418, in which it is markedly more curved and slenderer. Notably, *E. ferox*

displays a visible step at the craniomedial corner of the proximal articulation. The fovea capitis radii, a feature only visible in *E. khoikhoi*, is uniformly deep and round, with a well-defined articular circumference. The ulnar notch of *E. ferox* is wider and situated more distally, while in both MGPT-PU 135418 and *E. khoikhoi* it is smaller. The groove for the tendon of the extensor digitorum communis shows distinctions as well: in *E. ferox*, it is shallower and narrower, closely connected to the ulnar notch; whereas in *E. monticinensis*, MGPT-PU 135418 and *E. khoikhoi*, it is more elongated and distinct from the ulnar notch. In both *E. ferox* and *E. khoikhoi*, the ulnar proximal epiphysis is almost straight, with parallel anconeal and coronoid processes relative to the shaft; the lateral olecranon tuberosity is higher compared to that of the medial side. In contrast, *E. monticinensis* and MGPT-PU 135418 the ulnar proximal epiphysis is double-twisted with the olecranon area facing craniomedially and the proximal part of the shaft facing craniolaterally. In *E. ferox*, the ulna has a straight and wide shaft, and a slightly medially oriented styloid process. These elements are broken in *E. khoikhoi*. Conversely, *E. monticinensis* and MGPT-PU 135418, the ulna has a curve and thin shaft, and a straight styloid process.

Noteworthy differences are not readily apparent between the metacarpals, carpals, and phalanges of *E. khoikhoi*, *E. monticinensis*, and the Verduno specimen. As far as the available material is concerned, the metacarpal V of *E. monticinensis* is less curved and characterized by a wider distal articulation compared to that of MGPT-PU 135418.

### *Remarks*

Figure 8 and Supporting Information, Table S5 allow a comprehensive comparative analysis of the craniodental features in the genus *Eucyon*. The cranial morphology of MGPT-PU 135418 more closely resembles that of *E. davisii* than that of *E. ferox*, *E. zhoui*, *E. odessanus*, and *E. adoxus*. These species exhibit considerable similarities to each other, such as a long and slender splanchnocranium with a relatively long premaxilla, a long and bulging neurocranium, a sharp and prominent sagittal crest extending onto the frontals, and a subtriangular occipital squama. Notably, *E. khoikhoi* stands apart from the species mentioned above, exhibiting distinct characteristics, such as a weak sagittal crest, a wide nuchal crest, lyrate temporal crests merging into the sagittal crest in the final third of the braincase, and a semi-circular occipital squama. All these cranial characters align *E. khoikhoi* with foxes rather than with *Eucyon*. When observed in ventral view, MGPT-PU 135418 shows anteriorly convergent medial walls of the tympanic bullae, a condition

observed also in *E. davisii* and *E. ferox* (this condition is shared by the majority of *Vulpes* species; Bartolini-Lucenti and Rook 2021). Conversely, in *E. zhoui*, *E. adoxus*, and *E. khoikhoi*, these walls are parallel (as in many fossil *Canis* from Eurasia and North America; Bartolini-Lucenti and Rook 2021).

The mandibles of MGPT-PU 135418 resemble those of the species *E. davisii*, *E. minor*, *E. debonisi*, *E. odessanus*, *E. monticinensis*, *E. adoxus*, and *E. khoikhoi*, while they are rather different from those of *E. ferox*, *E. zhoui*, *E. marinae*, and *E. kuta*. In the first group, the corpus is slender with a (i) relatively curved (as seen in MGPT-PU 135418, *E. debonisi*, *E. monticinensis*, and *E. khoikhoi*) or (ii) straight (as observed in *E. davisii*, *E. minor*, *E. odessanus*, and *E. adoxus*) morphology. Additionally, the coronoid process is high and (i) tapered (in MGPT-PU 135418, *E. debonisi*, and *E. monticinensis*) or (ii) squared (as in *E. davisii*, *E. adoxus*, and *E. khoikhoi*). In contrast, the second group displays a robust and not tapered corpus, with a uniformly (i) curved (in *E. ferox* and *E. zhoui*) or (ii) straight (in *E. marinae* and *E. kuta*) ventral margin. Concerning the angular process, MGPT-PU 135418 exhibits similarities only to *E. minor* and *E. monticinensis* (slender and hook-shaped process), whereas species such as *E. ferox*, *E. adoxus*, and *E. khoikhoi* share a robust and hook-shaped process.

The upper premolars are rather conservative within the *Eucyon* species, including the Verduno fossil, except for *E. davisii* and *E. zhoui* whose P2 and P3 show a cusp-like distal cingulum, and *E. cipio*, with a P3 that bears a distal accessory cusp. In addition, *E. davisii* and *E. zhoui* are unique in lacking a crest connecting the P4 protocone with the paracone.

As far as the upper molars are concerned, *E. khoikhoi* stands out as the sole species without a pointed and well-developed M1 parastyle (this condition is shared by the majority of *Vulpes* spp.). In *E. ferox*, *E. zhoui*, *E. cipio*, *E. debonisi* (though notably reduced compared to others), and *E. adoxus*, the paracone is considerably larger than the metacone (a common trait within crown Canina; Tedford and Qiu 1996), whereas in all the other samples, these cusps are subequal in size. Notable differences in the protocone–metaconule connection can be observed in MGPT-PU 135418, *E. davisii*, *E. cipio*, *E. debonisi*, *E. monticinensis*, *E. odessanus*, and *E. khoikhoi* featuring a strong postprotocrista, while in *E. ferox*, *E. zhoui*, and *E. adoxus* the protocone is reduced and the metaconule is almost absent (or crest-like). The M1 paraconule is absent in *E. ferox*, *E. zhoui* (crest-like), and *E. khoikhoi*. As for the M2, *E. zhoui*, *E. cipio*, *E. odessanus*, *E. adoxus*, and *E. khoikhoi* exhibit subequal paracone and metacone. *Eucyon ferox*, *E. zhoui*,

*E. odessanus*, and *E. adoxus* lack a postprotocrista between the M2 protocone and metaconule. Additionally, the M2 paraconule is absent only in *E. ferox*, is poorly developed in *E. adoxus*, and is similarly underdeveloped in *E. khoikhoi*.

The lower premolars differ mostly in the shape of the distal cingulum and the presence/absence of distal accessory cuspids. Notably, p2 and p3 of MGPT-PU 135418, *E. minor*, *E. debonisi*, *E. monticinensis*, *E. odessanus* (which can exhibit a cuspid-like cingulum), and *E. kuta* lack distal accessory cuspids. Conversely, *E. davisii* and *E. marinae* (both of which can display a cuspid-like cingulum), *E. ferox*, *E. zhoui*, *E. adoxus*, and *E. khoikhoi* may exhibit accessory cuspids in these premolars. In p4, the presence of a second accessory cuspid distal to the first has been described as an autapomorphy of *Eucyon* shared with the ‘*Canis* group’ (i.e. crown Canina; Tedford and Qiu 1996). However, while in *Canis* this cuspid is fused to the distal cingulum (Bartolini-Lucenti and Rook 2021), in *E. davisii*, *E. ferox*, *E. marinae*, *E. debonisi*, *E. odessanus*, and *E. khoikhoi* it is clearly individualized from the well-developed distal cingulum. On the other hand, in MGPT-PU 135418, *E. zhoui*, *E. minor*, *Eucyon* sp. from Kvabebi, *E. monticinensis*, *E. adoxus*, and *E. kuta* the second distal accessory cuspid is still present, although very reduced (as in early species of *Canis*; Bartolini-Lucenti and Rook 2021) or partially fused with the mesial cuspid into a ridge (Werdelin *et al.* 2015).

As far as the lower molars are concerned, the m1 paraconid is robust and individualized from the protoconid in *E. ferox*, *E. cipio*, and *Eucyon* sp. from Mill-Langenboom; conversely, it is slender and adjacent to the protoconid in the remaining species and in MGPT-PU 135418. The metaconid is relatively small and adjacent to the protoconid in *E. ferox*, *E. cipio*, *Eucyon* sp. from Mill-Langenboom and Kvabebi, and *E. odessanus*. In addition, in *E. ferox* and *E. cipio*, the entoconid is cristid-like, whereas in *E. adoxus* it is subequal in size to the hypoconid. In all the other samples, the hypoconid is larger than the entoconid. The occlusal shape of m2 is trapezoid in all the analysed samples, except for *E. ferox*, *E. minor*, and *E. khoikhoi*, which possess a three-sided m2 shape, and *E. adoxus*, which exhibits a rounded m2. In all the species and in MGPT-PU 135418, the protoconid and the metaconid are subequal in size and aligned mesiodistally, except for *E. ferox*, *E. zhoui*, *E. marinae*, and *E. adoxus* in which the protoconid is much larger and placed more mesially than the metaconid (an apomorphic morphology reminiscent of that observed in crown Canina; Spassov and Rook 2006). In *E. ferox*, *E. marinae*, and *E. adoxus* the entoconid is not cristid-like. Only in *E. khoikhoi* are the

hypoconid and entoconid subequal in size. Finally, all m3s are oval in shape with the exception of *E. ferox* and *E. khoikhoi*, which possess almost circular m3s in occlusal view.

Finally, regarding the postcranial skeleton, we detected several differences in the humerus, radius, and ulna of MGPT-PU of *E. monticinensis*. However, these results should be regarded as tentative given the limited comparative information available for postcranial remains of *Eucyon*.

### Biometric comparisons

In this section, linear measurements of the cheek teeth are used to create log<sub>10</sub> ratio diagrams and bivariate plots aimed at identifying similarities and differences in absolute sizes and proportions between the Verduno specimen and numerous *Eucyon* samples (see Supporting Information, Tables S6–S8)

In the analysis of the upper teeth, *E. ferox* and *E. cipio* on the one hand and *E. debonisi* and *E. khoikhoi* on the other are confirmed to be the largest and the smallest *Eucyon* species, respectively (Fig. 9). This is confirmed by body mass estimates based on m1 length (Table 4). In the log<sub>10</sub> ratio diagram (Fig. 9), *E. ferox*, *E. davisii* from North America, and *E. odessanus* exhibit a similar trend, except for P4 length in *E. ferox* and width of M1 in *E. odessanus*, which are relatively smaller. The pattern of MGPT-PU 135418 closely resembles that of *E. debonisi* in the general trend, but the latter has considerably smaller upper teeth. The dental proportions of MGPT-PU 135418 are also similar to those of *E. davisii*, although the *Eucyon* from Verduno has wider premolars than North American *E. davisii* and overall larger molars than both North American and Asian samples of the species. The pattern of *E. adoxus* closely resembles that of the standard *C. aureus*, except for the overall smaller P2 and P3 and longer M1 and M2; in these features, *E. adoxus* differs from the other *Eucyon*, despite some similarities with *E. khoikhoi* and *E. zhoui* (Fig. 9).

In the bivariate plots of width against length of P4 (Fig. 9A2), MGPT-PU 135418 falls within the range of North American and Asian *E. davisii* and in the lower part of the range of *E. zhoui*. Both *E. zhoui* and *E. adoxus* exhibit a wider P4, while that of *E. odessanus* is relatively longer. In the M1 bivariate plots (Fig. 9A3), the wide range of variation of *E. davisii* is even more evident. As far as concerns P4, the Verduno specimen falls about in the middle of this range. M1 of MGPT-PU 135418 is located between the two available teeth of *E. monticinensis*, within the ranges of *E. zhoui* and *E. odessanus*,

and close to that of *E. adoxus* (which has longer M1s on average). The measurements of *E. debonisi* and *E. khoikhoi* overlap with the smallest values of *E. davisii* (Fig. 9).

Looking at the log10 ratio diagram of the lower teeth (Fig. 9B1), the trends can be divided into two groups. The first is exemplified by *E. ferox* (although its m2 length is significantly smaller), *E. marinae*, *E. zhoui*, *E. minor*, and *E. cipio* (for which only the m1 is available), all of which have significantly larger lower teeth. The second group includes *E. odessanus*, *E. davisii*, *E. monticinensis*, the Verduno specimen, *E. khoikhoi* (although its m1 is relatively shorter), and *E. debonisi*. In particular, the pattern of MGPT-PU 135418 falls between those of *E. monticinensis* and *E. debonisi*. *Eucyon adoxus* closely aligns with the standard pattern (extant *C. aureus*), except for the notably wide p4 (see also the bivariate plot in Fig. 9B2). The African *E. kuta* stands out for the different proportions of the premolars compared to all the other taxa (Fig. 9B1).

The p4 bivariate plot allows the different taxa to be distinguished quite clearly (Fig. 9B2). The p4 of *E. kuta* is about as short as those of *E. debonisi* and *E. khoikhoi*, but wider. *Eucyon ferox* and *E. marinae* have p4s that are considerably larger than those of the other taxa. *Eucyon davisii* exhibits the widest range of variation, which encompasses that of *E. odessanus* and the only known record of *E. monticinensis*. The p4 of MGPT-PU 135418 falls in the lower part of the *E. davisii* range, close to the largest *E. khoikhoi* and *E. debonisi* specimens. The p4s of *E. zhoui* and *E. minor* are, respectively, wider and longer than those of *E. davisii*. A larger number of records were available for the comparative analysis of the size of m1 (Fig. 9B3). Again, the wide range of *E. davisii* encompasses those of many other taxa. The m1 of MGPT-PU 135418 is placed in the middle of this range in terms of length, and in its upper part in terms of width, also falling within the range of *E. monticinensis* and close to those of *E. zhoui*, *E. adoxus*, and *E. minor*.

In terms of body mass estimates (Table 4), the Verduno specimen aligns with *E. davisii*, *E. monticinensis*, *E. odessanus*, and *E. zhoui*, all showing an average body mass of 11 kg. *Eucyon adoxus*, *E. marinae*, and *E. minor* are slightly larger (12 kg), whereas *E. kuta* and *E. debonisi* are slightly smaller (10 and 9 kg, respectively). *Eucyon cipio* and *E. ferox* stand out for their high body mass (15 kg), whereas *E. khoikhoi* is smaller than the other taxa (8 kg).

### **Endocranial anatomy**

The brain endocast of the specimen from Verduno is slightly larger than that of *E. davisii* although both show considerable similarities in terms of proportions and general arrangement of the sulcal pattern (see Fig. 6 and Supporting Information, Table S4). Comparison with extant canids reveals a strong resemblance between the cerebrum of *Eucyon* and those of *V. vulpes*, *C. aureus*, *C. latrans*, and *L. mesomelas*, with some relevant differences in the sulcal pattern, as already pointed out by Lyras (2009). Moving from the front to the back, the proreal gyrus in *Eucyon* is shorter and bilaterally constricted compared to that of extant canids of similar size. The outline and expansion of the sigmoid gyrus of *Eucyon* is comparable to that of *Vulpes* but is reduced compared to those of other canids. The cruciate and posterucuate sulci of MGPT-PU 135418 are not discernible, while in *E. davisii* they are well developed (Lyras 2009). In *E. davisii*, the ansate sulcus is shorter compared to the Verduno specimen, in which it is quite well developed and resembles that of *Vulpes*. In lateral view, the region corresponding to the frontal pole cortex appears flattened in MGPT-PU 135418 and *E. davisii*, whereas in all present-day canids this portion of the cerebrum shows a significant dorsoventral swelling. The lateral and ectolateral sulci of *Eucyon* show a similar disposition to that of extant canids, albeit the ectolateral sulcus is not connected to the suprasylvian sulcus. In MGPT-PU 135418 and *E. davisii* F:AM 63005 reported by Lyras (2009), the endolateral sulcus being missing, despite the presence of a very shallow endolateral sulcus is noticeable on specimen F:AM 97057 of *E. davisii*.

Concerning the frontal sinuses, those of MGPT-PU 135418 are large and well developed, morphologically and in dimensions similar to those of *E. davisii*, but of greater volume (Fig. 10; Supporting Information, Table S3). The frontal sinuses of *E. adoxus* differ from those of *E. monticinensis* and *E. davisii* by having a more pronounced and laterally directed rostromedial lobe. In general, the specimens of *Eucyon* considered in this work would appear to have larger frontal sinuses compared to fossil and extant canids of a similar or even greater size, such as *C. arnensis*, *C. aureus*, *C. latrans*, *L. mesomelas*, *L. sadusta*, *Canis simensis*, and *C. lupaster*, and considerably smaller to those of *C. etruscus*, *C. lupus*, and *L. pictus*. However, in a specimen of *L. pictus* (MC438) the frontal sinuses are considerably reduced in size and volume compared to those of *Eucyon*. Small frontal sinuses in *L. pictus* also were documented by Curtis *et al.* (2018). In small-sized canids such as *Speothos venaticus* Lund (1842), *Vulpes lagopus* Linnaeus, 1758, and *V. vulpes*, frontal sinuses are strongly reduced or even absent (Tedford *et al.* 2009, Curtis

and Van Valkenburgh 2014, Frosali *et al.* 2023). In the only specimen of *S. venaticus* examined for comparative purposes (MC266), we detected the presence of reduced frontal sinuses, as also documented by Huxley (1880), whose observation was based on a single specimen, as in our case. In contrast, Van Valkenburgh *et al.* (2014) reported an absence of frontal sinuses in the single specimen of *S. venaticus* they examined. *Vulpes vulpes* is commonly considered a canid without frontal sinuses, but in two specimens examined herein (MC70, MC96) they are present and relatively developed. Frontal sinuses in *V. vulpes* also were documented by Mahdy and Zayed (2020). When present, the frontal sinuses of *Speothos* and *Vulpes* always appear much smaller and morphologically different from those of *Eucyon*. These pieces of evidence suggest that frontal sinuses may be affected by intraspecific variability, not only in terms of size and morphology, but also in terms of presence/absence.

### Phylogenetic relationships

Our phylogenetic analysis resulted in two equally parsimonious trees of 198 steps, consistency index of 0.460 and retention index of 0.592. The strict consensus tree is shown in Figure 11. The distribution of character states in the most parsimonious trees is reported in Supporting Information, Appendix S2.

The basal position of the extant Vulpini, *V. vulpes* and *N. procyonoides*, is consistent with previous phylogenetic analyses based on morphological and/or molecular data, although it should be pointed out that the systematics of the Vulpini and the phylogenetic relationships between *Vulpes* and *Nyctereutes* are subject to controversies in the literature (see: Bartolini-Lucenti *et al.* 2018). In the analysis by Prevosti (2010: fig. 4), the Vulpini are paraphyletic and *V. vulpes* is basal to *N. procyonoides*, as in our tree. A similar result was obtained by Zrzavý *et al.* (2018: fig. 1a) when both morphological and molecular data are considered. On the contrary, when only DNA data are analysed, the Vulpini form a monophyletic clade, with *Nyctereutes* as the most basal taxon (Wayne and Ostrander 2007). The position of *E. khoikhoi* in the tree (Node 6) raises some questions. According to the paper by Valenciano *et al.* (2021) in which the species was described, *E. khoikhoi* was regarded as the most basal taxon of an ‘African clade’ including also *E. wokari*, *?Nyctereutes barryi* (Werdelin and Dehghani 2011), *?Schaeffia mohibi* (= *Lupulella mohibi* in Geraads, 2011), and the extant side-striped jackal *Schaeffia adusta* (= *L. adusta* in this paper). This African clade was interpreted to be sister to that of ‘true’ *Eucyon*, which is the clade of *E. davisi*, *E. debonisi*, and *E. ferox* (Valenciano *et al.*, 2021). On the

other hand, our analysis shows a certain phylogenetic proximity between *E. khoikhoi* and the Vulpini, to which this species could belong. Indeed, numerous morphological characters highlighted in our comparative analysis (e.g. condylobasal length, concave dorsal surface of the postorbital process of the frontal, and shape and development of the temporal crests; see ‘Remarks’ in the Morphological comparisons section above) seem to align this South African species more with foxes than with *Eucyon*.

Node 23 includes extant and extinct Canini and is supported by nine synapomorphies (Supporting Information, Appendix S2). The clade is divided into two monophyletic groups. The first (Node 22) is the *Eucyon* clade, in which *E. davisii* is the most basal taxon, followed by *E. monticinensis* and then by the pair formed by the Chinese *E. zhoui* and the European *E. adoxus*. This topology is consistent with stratigraphic information, as *E. davisii* is the earliest known species of the genus, *E. monticinensis* occurs in the fossil record since the Late Miocene, while both *E. zhoui* and *E. adoxus* are not known before the Early Pliocene (see Fig 1 for a summary). The second clade of Canini (Node 27) has *E. ferox* in the basal position. The sister-group relationship between this North American species and crown-Canini is noteworthy, and it was retrieved also in other phylogenetic analyses (i.e. Tedford *et al.* 2009, Zrzavý *et al.* 2018). Since its first description (Miller and Carranza-Castañeda 1998), *E. ferox* has long been. Only recently, Bartolini-Lucenti and Rook (2021) suggested moving *C. ferox* within the genus *Eucyon* based on selected cranial and dentognathic features. Our results reopen the issue of the systematics of this taxon, which indeed seems to show a suite of intermediate characters between *Eucyon* and crown-Canini.

In the crown-Canini clade (Node 31), the sister-taxon relationships between the extant African jackals *L. adusta* and *L. mesomelas* are consistent with the majority of the available studies based on morphological or molecular datasets (Lindblad-Toh *et al.* 2005, Prevosti 2010, Koepfli *et al.* 2015, Zrzavý *et al.* 2018, Perri *et al.* 2021). The jackal clade is the sister-group of the clade of ‘wolf-like’ canids. According to molecular data (Koepfli *et al.* 2015, Gopalakrishnan *et al.* 2018, Perri *et al.* 2021), the extant species of *Canis* should have diverged in the following order: *C. aureus*–*C. lupaster*–the pair formed by *C. latrans* and *C. lupus*. In our tree, this model is substantially respected, except for the sister-group relationship retrieved between *C. aureus* and *C. lupaster* (Node 35). This result might be explained by the fact that these two species in fact share a very similar morphology, to the point that for a very long time they were considered as a single species,

*C. aureus* [see historical overview in Viranta *et al.* (2017)]. The Early Pleistocene species *C. arnensis* (Node 29) and *C. etruscus* (Node 28) precede the wolf plus coyote clade (Node 33). This is fully consistent with the phylogenetic analysis by Tedford *et al.* (2009), as well as with other palaeontological studies suggesting that *C. arnensis* would show more similarities with the golden jackal (Bartolini-Lucenti and Rook 2016) and *C. etruscus* with the wolf (Cherin *et al.* 2014). The polytomy between *C. lupus*, *A. dirus*, and *L. pictus* (Node 32) contrasts with the molecular data, based on which the Middle–Late Pleistocene *A. dirus* should be basal to crown-Canini, whereas the extant wild dog should be basal to the *Canis* clade (Lindblad-Toh *et al.* 2005, Koepfli *et al.* 2015, Perri *et al.* 2021). However, the three species show strong phenotypic convergence related to their hypercarnivorous diet, so much so that they always cluster close to each other in phylogenetic trees based on morphological characters (Tedford *et al.* 2009, Prevosti 2010: Figs 1, 3).

## CONCLUSION

Based on the thorough morphological and biometric comparisons between the cranial and postcranial material presented herein, the assignment of MGPT-PU 135418 to *E. monticinensis* is strongly supported (Fig. 12; Supplementary Information, video).

The outstanding skeleton from Verduno significantly improves our knowledge of the early diffusion of *Eucyon* in Europe. The earliest representative of this genus on the continent is the enigmatic *E. cipio*, which is represented by only a few teeth from Spain. Consequently, its taxonomic status and phylogenetic relationships remain uncertain. Our results indicate that *E. cipio* is quite distinct from other members of the genus in both morphology and size. Therefore, as pointed out by Rook (2009), it is possible that *E. cipio* may belong to an earlier westward dispersal of Canini into Europe, possibly even closer to the differentiation of the genus *Canis*.

The first ‘true’ *Eucyon* species in Europe are *E. monticinensis* and *E. debonisi*, both occurring in the Messinian (MN13 and MN14) of Italy and Spain (a few remains of the former species are also reported from the earliest Pliocene of southern Spain; Piñero *et al.* 2017). Although the material from the type localities (Brisighella and Venta del Moro, respectively) is quite abundant, the crania of these two species remained largely unknown before the discovery of the Verduno specimen described herein. The mandibles and teeth of *E. monticinensis* and *E. debonisi* share several similarities. As a matter of fact, *E.*

*debonisi* differs from *E. monticinensis* only in its smaller size and some subtle dental features. On that basis, we suggest that *E. debonisi* should be considered a junior synonym of *E. monticinensis*, as previously advocated by Rook (1992) and Sotnikova and Rook (2010).

Although well-preserved crania of *Eucyon* are very few, it is evident that the specimen from Verduno resembles *E. davisi* in several aspects (e.g. general morphology of the cranium, relative development of neurocranium and splanchnocranium, shape of the occipital region, brain and frontal sinus anatomy). In contrast, more derived species, such as *E. zhoui* and *E. adoxus*, exhibit larger overall size, more elongated and slender muzzles, relatively wider zygomatic arches, stronger sagittal crest, and dental characters closer to the typical morphology of *Canis*.

From a phylogenetic perspective, Tedford and Qiu (1996) regarded *Eucyon* as a paraphyletic group. The scarcity of fossils available for many *Eucyon* samples and the objectively reduced morphological variability within and between the Caninae make this issue difficult to unravel. For example, *E. adoxus* was previously assigned to the genus *Vulpes* Frisch (1975) (Pons-Moya and Crusafont-Pairò 1978) (Supporting Information, Appendix S1). Conversely, *E. cipio* and *E. ferox* were initially referred to *Canis* but are now generally recognized as members of *Eucyon* (Rook 2009, Bartolini-Lucenti *et al.* 2021). The few available phylogenetic data are also contradictory. *Eucyon davisi* is generally accepted as one of the earliest Canini. In contrast, according to Zrzavý *et al.* (2018), *E. marinae* and *E. zhoui* should be close to the origin of crown-Canini (but the extremely poor record of the former species makes its inclusion in a phylogenetic analysis rather problematic). The inferred phylogenetic position of *E. ferox* ranges from very basal in the clade that includes *Canis* (Tedford *et al.* 2009, Zrzavý *et al.* 2018) to derived in a clade also including *E. davisi* and *E. debonisi* Valenciano *et al.* (2022). According to Valenciano *et al.* (2022), the South African *E. khoikhoi* would occupy the most basal position among the African canines, in a clade including also ‘*E.*’ *wokari*, ?*Nyctereutes barryi*, *L. mohibi*, and the extant side-striped jackal. They also propose that (i) the Late Miocene ‘*E.*’ *intrepidus* from Kenya may also belong to this clade; (ii) the Late Pliocene *E. kuta* from Ethiopia could be phylogenetically closer to the black-backed jackal; and (iii) *E. cipio* would be the sister group of *C. lupus* (Valenciano *et al.*, 2021). Again, it is worth pointing out that the inclusion in phylogenetic analyses of species represented by very poor fossil

records, such as '*E.* *wokari* and *E. cipio* (Supporting Information, Appendix S1), might lead to misleading results.

Unlike the aforementioned studies, in our phylogenetic analysis we only considered samples for which sufficiently complete cranial and postcranial remains were available. In our tree (Fig. 11), *E. davisii* is basal in a monophyletic group also including *E. monticinensis* and the sister-taxa *E. adoxus* and *E. zhoui*. The phylogenetic position of *E. khoikhoi* would suggest its possible attribution to the Vulpini, as supported by its numerous fox-like cranial characters (e.g. weak sagittal crest, wide and downwardly directed nuchal crest that does not extend more caudally than the occipital condyles, and lyrate sagittal crest; see also Supporting Information, Table S5). Similarly, our phylogenetic results could lead to a reconsideration of the systematic status of *E. ferox*, which is basal to crown-Canini and shows several *Canis*-like features (e.g. sharp medial indentation at the interorbital constriction, paracone of M2 markedly enlarged, presence of a posterior second accessory cuspid in p4, and hypoconid much larger than the entoconid in the m1; see also Supporting Information, Table S5). However, a more detailed discussion on the systematics of *E. khoikhoi* and *E. ferox* (as well as on the phylogenetic relationships of crown-Canini) is beyond the scope of this manuscript but may serve as a starting point for future investigations.

Regarding endocranial morphology, we agree with Lyras (2009) in considering the brain of *Eucyon* to be more primitive than those of crown-Canini, and more similar to those of Vulpini. In particular, the flattening of the frontal pole cortex observed in *E. monticinensis* and *E. davisii* appears to be a character shared with some present-day foxes such as *Vulpes bengalensis* (Shaw, 1800), *Vulpes rueppellii* Schinz, 1825, *Vulpes chama* (Smith, 1833), and *Vulpes zerda* Zimmermann, 1780 [see Lyras (2009: fig. 27)]. However, it is not clear if in *Eucyon* this brain morphology is related to the presence of large frontal sinuses, as in foxes these are poorly developed or even absent. In addition, the frontal cortex is known to mediate complex social behaviour in primates (Dunbar and Bever 1998; Dunbar 2003) and probably in other mammals such as canids (Radinsky 1969) and spotted hyenas (Holekamp *et al.* 2007, Sakai *et al.* 2011, Vinuesa *et al.* 2016). If so, it would be plausible to assume that *E. monticinensis* and *E. davisii* were not equipped to express complex social behaviours, thus excluding that they were pack-hunting species.

Although the function of the frontal sinuses in canids, and more generally in mammals, is still unclear and a matter of debate, some authors suggest that they might

have a possible role in bite biomechanics and feeding habits (e.g. Paulli 1900, Curtis and Van Valkenburgh 2014, Curtis *et al.* 2018). In a recent study, Frosali *et al.* (2023) analysed the frontal sinuses of several extant canids and three species of *Eucyon* indicating a correlation with three ecomorphotypes (hypercarnivores, mesocarnivores, and hypocarnivores), with *E. adoxus* falling in the category of hypercarnivorous canids and *E. davisii* showing affinity with mesocarnivorous canids. Although a detailed analysis of the biomechanics of the skull is beyond the scope of this work, in our opinion the use of ecomorphotypes is questionable. Hypercarnivory indicates a diet based 70% on meat, but offers no information on prey size, on mechanics of prey capture, or the ratio of hard parts (bones) to soft tissue consumed, which are also affected by environmental conditions and seasonality. For instance, in *S. venaticus*, an hypercarnivorous group-hunting canid, the frontal sinuses are strongly reduced or absent, and the same applies to some specimens of *L. pictus*, suggesting that the correlation between frontal sinuses and ecomorphotypes should be approached with caution. There are probably many factors involved in shaping the frontal sinuses of canids such as ontogeny, intraspecific variability, and food texture (Curtis *et al.* 2018) that need to be further explored. Based on current knowledge and the data obtained from this study, it is difficult to ascribe the species of *Eucyon* to specific ecomorphotypes.

Considering the partial skeleton of *E. monticinensis* from Verduno, including the external and internal features of the skull and the inferred body mass, this species was probably capable of hunting lagomorph-sized prey, as well as feeding on plant material, insects, and other foods sources in an opportunistic way. Given the similarities between *E. monticinensis* and *E. davisii*, it is reasonable to infer that the latter species had similar ecological characteristics to the former. In contrast, based on the shape of the skull, teeth, and frontal sinuses, we agree with the interpretation suggested by Frosali *et al.* (2023) in recognizing *E. adoxus* as a small-prey hunter.

## **SUPPLEMENTARY DATA**

Supplementary data are available at *Zoological Journal of the Linnean Society* online.

## **ACKNOWLEDGEMENTS**

The early stages of this work were supported by two Erasmus + traineeships in the Swedish Museum of Natural History granted to the first author. The authors would like

to sincerely thank the following people: Álvaro López for his collaboration in the preparation of the specimen during his traineeship at the Department of Physics and Geology, University of Perugia; Francesco Porciello and Giovanni Angeli (University of Perugia) for the first attempts of analysing the Verduno specimen by medical CT; Sofia Menconero for her unvaluable support in the making of and analysis of the 3D models; Qigao Jiangzuo for pictures of *Eucyon* from the American Museum of Natural History; Lorenzo Rook for data on *E. monticinensis* from Brisighella; George Lyras for sharing the 3D model of the brain endocast of *E. davisii* (F:AM 97057); Elisabetta Cioppi for having granted access to the collections of the Museum of Geology and Paleontology, University of Florence; David Alba (Institut Català de Paleontologia Miquel Crusafont) and the staff of the museum in Sabadell for having granted access to the material of *E. cipio*. Two anonymous reviewers are deeply acknowledged for their work. This is the publication number 379 of the Museo di Geologia e Paleontologia collections at the Università degli Studi di Torino.

#### **CONFLICT OF INTEREST**

The authors declare that they have no conflicts of interest in relation to this work.

#### **DATA AVAILABILITY**

The data underlying this article are available in the article and in its online Supporting Information.

#### **REFERENCES**

Abbazzi L. Cervidae and Moschidae (Mammalia, Artiodactyla) from the Baccinello V3 faunal assemblage (Late Miocene, Late Turolian, Grosseto, Central Italy). *Rivista Italiana di Paleontologia e Stratigrafia* 2001;**107**:10–123.

Abbazzi L, Benvenuti M, Boschian G *et al.* Revision of the Neogene and Pleistocene of the Gargano region (Apulia, Italy). The marine and continental successions and the mammal faunal assemblages in an area between Apricena and Poggio Imperiale (Foggia). *Memorie della Società Geologica Italiana* 1996;**51**:383–402.

Abbazzi L, Delfino M, Gallai G *et al.* New data on the vertebrate assemblage of Fiume Santo (North-West Sardinia, Italy), and overview on the late Miocene Tusco-Sardinian palaeobioprovince. *Palaeontology* 2008;**51**:425–51.<https://doi.org/10.1111/j.1475-4983.2008.00758.x>

Agisoft LLC. *Agisoft Photoscan Pro*. St. Petersburg: Russia, 2014. Available online: <http://www.agisoft.com> (accessed on 15 November 2022).

Artec 3D. *Artec Europe. Artec Space Spider*. Available online: <https://www.artec3d.com/de/portable-3d-scanners/artec-spider-v2> (accessed on 6 November 2020).

Balisi M, Wang X, Sankey J *et al*. Fossil canids from the Mehrten Formation, late Cenozoic of northern California. *Journal of Vertebrate Paleontology* 2018;**38**:e1405009. <https://doi.org/10.1080/0272463.4.2017.1405009>

Bartolini-Lucenti S, Rook L. A review on the Late Villafranchian medium-sized canid *Canis arnensis* based on the evidence from Poggio Rosso (Tuscany, Italy). *Quaternary Science Reviews* 2016;**151**:58–71.

Bartolini-Lucenti S, Rook L. ‘*Canis*’ *ferox* Revisited: diet ecomorphology of some long gone (Late Miocene and Pliocene) Fossil Dogs. *Journal of Mammalian Evolution* 2021;**28**:285–306.

Bartolini-Lucenti S, Rook L, Morales J. *Nyctereutes* (Mammalia, Carnivora, Canidae) from Layna and the Eurasian raccoon-dogs: an updated revision. *Rivista Italiana di Paleontologia e Stratigrafia* 2018;**124**:597–616.

Bartolini-Lucenti S, Madurell-Malapeira J, Rook L. I carnivori di Cava Monticino (Brisighella, RA). In: Rook L (ed.), *La Fauna Messiniana di Cava Monticino (Brisighella, RA). Memorie dell’Istituto Italiano di Speleologia Serie II-Vol. 37*, 2021, 133–49. Società Speleologica Italiana: Bologna.

Bartolini-Lucenti S, Madurell-Malapeira J, Rook L. The carnivorans from Cava Monticino (Faenza, Italy; Messinian) revisited. *Historical Biology* 2022;**34**:1458–70. <https://doi.org/10.1080/08912963.2022.2042806>

Batsch AJGC. *Versuch Einer Anleitung, Zur Kenntniß und Geschichte der Thiere und Mineralien, Für Akademische Vorlesungen Entworfen und Mit den Nöthigsten Abbildungen Versehen*. Erster Theil. Jena: Akademischen Buchhandlung, 1788.

Benvenuti M, Papini M, Rook L. Mammal biochronology, UBSU and paleoenvironment evolution in a post-collisional basin: evidence from the Late Miocene

Baccinello-Cinigiano basin in southern Tuscany, Italy. *Bollettino della Società Geologica Italiana* 2001;**120**:97–118.

Bernor RL, Fortelius M, Rook L. Evolutionary biogeography and paleoecology of the ‘*Oreopithecus bambolii* Faunal Zone’ (Late Miocene, Tusco-Sardinian Province). *Bollettino della Società Paleontologica Italiana* 2001;**40**:139–48.

Bowdich TE. *An Analysis of the Natural Classifications of Mammalia, for the Use of Students and Travellers*. Paris: J. Smith, 1821.

Carnevale G, Gennari R, Lozar F *et al.* Living in a deep desiccated Mediterranean Sea: an overview of the Italian fossil record of the Messinian salinity crisis. *Bollettino della Società Paleontologica Italiana* 2019;**58**:109–40.

Cavallo O, Sen S, Rage JC *et al.* Vertébrés messiniens du Faciès à congéries de Ciabòt Cagna, Corneliano d’Alba (Piémont, Italie). *Rivista Piemontese di Storia Naturale* 1993;**14**:3–22.

Cherin M, Bertè DF, Rook L *et al.* Re-defining *Canis etruscus* (Canidae, Mammalia): a new look into the evolutionary history of Early Pleistocene dogs resulting from the outstanding fossil record from Pantalla (Italy). *Journal of Mammalian Evolution* 2014;**21**:95–110. <https://doi.org/10.1007/s10914-013-9227-4>

Cignoni P, Callieri M, Corsini M, *et al.* MeshLab: an open-source mesh processing tool. In: Scarano V, De Chiara R (eds), *Eurographics Italian Chapter Conference*, 2008;129–36.

Colombero S, Bonelli E, Kotsakis A *et al.* Late Messinian rodents from Verduno (Piedmont, NW Italy): biochronological, paleoecological and paleobiogeographical implications. *Geobios* 2013;**46**:111–25.

Colombero S, Angelone C, Bonelli E *et al.* The upper Messinian assemblages of fossil vertebrate remains of Verduno (NW Italy): another brick for a latest Miocene bridge across the Mediterranean. *Neues Jahrbuch für Geologie und Paläontologie—Abhandlungen* 2014;**272**:287–324. <https://doi.org/10.1127/0077-7749/2014/0408>

Colombero S, Pavia M, Carnevale G. Old World porcupine (Rodentia, Hystricidae) remains from the late Messinian of Piedmont, NW Italy. *Rivista Italiana di Paleontologia e Stratigrafia* 2015;**121**:243–53.

Colombero S, Alba DM, D'Amico C *et al.* Late Messinian mollusks and vertebrates from Moncucco Torinese, north-western Italy. *Paleoecological and Paleoclimatological Implications. Palaeontologia Electronica* 2017a;**20**:1–66.

Colombero S, Bonelli E, Pavia M *et al.* *Paracamelus* (Mammalia, Camelidae) remains from the late Messinian of Italy: insights into the last camels of Western Europe. *Historical Biology* 2017b;**29**:509–18. <https://doi.org/10.1080/08912963.2016.1206539>

Crusafont Pairó M. El primer representante del género *Canis* en el Pontiense Euroasiático (*Canis cipio* n. sp.). *Boletín de la Real Sociedad Española de Historia Natural* 1950;**48**:43–51.

Curtis AA, Van Valkenburgh B. Beyond the sniffer: frontal sinuses in Carnivora. *Anatomical Record (Hoboken, N. J.: 2007)* 2014;**297**:2047–64. <https://doi.org/10.1002/ar.23025>

Curtis AA, Orke M, Tetradis S *et al.* Diet-related differences in craniodental morphology between captive-reared and wild coyotes, *Canis latrans* (Carnivora: Canidae). *Biological Journal of the Linnean Society* 2018;**123**:677–93. <https://doi.org/10.1093/biolinnean/blx161>

De Giuli C, Masini F, Torre D. The mammal fauna of the Monticino quarry. In: De Giuli C, Vai GB (eds), *Guide Book of the Workshop 'Continental Faunas at the Mio-Pliocene Boundary'*. 1988, 65–9. Società Paleontologica Italiana: Faenza.

Dela Pierre F, Festa A, Irace A. Interaction of tectonic, sedimentary and diapiric processes in the origin of chaotic sediments: an example from the Messinian of the Torino Hills (Tertiary Piedmont Basin, northwestern Italy). *Geological Society of America Bulletin* 2007;**119**:1107–19. <https://doi.org/10.1130/b26072.1>

Dela Pierre F, Bernardi E, Cavagna S *et al.* The record of the Messinian salinity crisis in the Tertiary Piedmont Basin (NW Italy): the Alba section revisited. *Palaeogeography, Palaeoclimatology, Palaeoecology* 2011;**310**:238–55. <https://doi.org/10.1016/j.palaeo.2011.07.017>

Del Campana D. I cani pliocenici di Toscana. *Palaeontographia Italica* 1913;**19**:189–254.

Dunbar RIM. The social brain: mind, language, and society in evolutionary perspective. *Annual Review of Anthropology* 2003;**32**:163–81. <https://doi.org/10.1146/annurev.anthro.32.061002.093158>

Dunbar RIM, Bever J. Neocortex size predicts group size in carnivores and some insectivores. *Ethology* 1998;**104**:695–708. <https://doi.org/10.1111/j.1439-0310.1998.tb00103.x>

Ezquerro L, Luzón A, Simón JL *et al.* A review of the European Neogene Mammal zones from integration of litho-, bio- and magnetostratigraphy in the Teruel Basin. *Earth-Science Reviews* 2022;**234**:104223. <https://doi.org/10.1016/j.earscirev.2022.104223>

Faggi A, Bartolini-Lucenti S, Rook L. New insights on the enigmatic otters from the Late Micene of Tuscany: Tyrrhenolutra maremmana nov. comb. (Lutrinae, Mustelidae, Carnivora), with a phylogeny of bunodont otters. *Rivista Italiana di Paleontologia e Stratigrafia* 2024;**130**:259—84.

Fedorov A, Beichel R, Kalpathy-Cramer J *et al.* 3D Slicer as an image computing platform for the quantitative imaging network. *Magnetic Resonance Imaging* 2012;**30**:1323–41. <https://doi.org/10.1016/j.mri.2012.05.001>

Ferretti MP, Rook L, Torre D. *Stegotetrabelodon* cf. *syrticus* (Proboscidea, Elephantidae) from the Upper Miocene of Cessaniti (Calabria, southern Italy) and its bearing on Late Miocene paleogeography of central Mediterranean. *Journal of Vertebrate Paleontology* 2003;**23**:659–66. <https://doi.org/10.1671/2353>

Forsyth Major CI. Considerazioni sulla fauna dei Mammiferi pliocenici e postpliocenici della Toscana. III. Cani fossili del Val d'Arno superiore e della Valle dell'Era. *Atti della Società Toscana di Scienze Naturali* 1877;**3**:207–27.

Frisch JL. *Das Natur-System der Vierfüßigen Thiere in Tabellen, Darinnen alle Ordnungen, Geschlechter und Arten, Nicht Nur mit Bestimmenden Benennungen, Sondern Beygesetzten unterscheidenden Kennzeichen Angezeigt Werden zum Nutzen der Erwachsenen Schuljugend.* Głogów: C.F. Günther, 1975.

Frosali S, Bartolini-Lucenti S, Madurell-Malapeira J *et al.* First digital study of the frontal sinus of stem-Canini (Canidae, Carnivora): evolutionary and ecological insights throughout advanced diagnostic in paleobiology. *Frontiers in Ecology and Evolution* 2023;**11**:1173341.

Gallai G, Rook L. *Propotamochoerus* sp. (Suidae, Mammalia) from the late Miocene of Gravitelli (Messina, Sicily, Italy) rediscovered. *Rivista Italiana di Paleontologia e Stratigrafia* 2006;**112**:317–21.

García N. New *Eucyon* remains from the Pliocene Aramis Member (Sagantole Formation), Middle Awash Valley (Ethiopia). *Comptes Rendus Palevol* 2008;**7**:583–90. <https://doi.org/10.1016/j.crpv.2008.10.005>

Gaspard M. La région de l'angle mandibulaire chez les Canidae. *Mammalia* 1964;**28**:249–329. <https://doi.org/10.1515/mamm.1964.28.2.249>

Gervais P. Sur un singe fossile d'une espèce non encore décrite, qui a été découverte au Monte Bamboli. *Comptes Rendus Hebdomadaires des Séances de l'Académie de Sciences de Paris* 1872;**74**:1217–23.

Ghibaud G, Clari P, Perello M. Litostratigrafia, sedimentologia ed evoluzione tettonico-sedimentaria dei depositi miocenici del margine sud-orientale del Bacino Terziario Ligure-Piemontese (Valli Borbera, Scrivia e Lemme). *Bollettino della Società Geologica Italiana* 1985;**104**:349–97.

Ginsburg L. Order Carnivora. In: Rössner GE, Heissig K (ed.), *The Miocene Land Mammals of Europe*. München: Verlag Dr. Friedrich Pfeil, 1999, 109–48.

Girardeau-Montaut D. CloudCompare (version 2.12. 4). *GPL Software* 2020.<http://cloudcompare.org>

Goloboff PA, Morales ME. TNT version 1.6, with a graphical interface for MacOS and Linux, including new routines in parallel. *Cladistics* 2023;**39**:144–53. <https://doi.org/10.1111/cla.12524>

Gopalakrishnan S, Sinding MHS, Ramos-Madrugal J *et al.* Interspecific gene flow shaped the evolution of the genus *Canis*. *Current Biology* 2018;**29**:4152–3449. <https://doi.org/10.1016/j.cub.2019.11.009>

Gray JE. *Illustrations of Indian Zoology: Chiefly Selected from the Collection of Major General Hardwicke*. London: Adolphs Richter & Co. and Parbury, Allen & Co, 1834.

Haile-Selassie Y, Howell FC. Carnivora. *Ardipithecus kadabba late miocene evidence from the middle awash. Ethiopia* 2012;**8**:237–75. <https://doi.org/10.1525/california/9780520254404.003.0008>

Hilzheimer M. Die geographische Verbreitung der Afrikanischen Grauschakale. *Zoologischer Beobachter* 1906;**47**:363–73.

Holekamp KE, Sakai ST, Lundrigan BL. Social intelligence in the spotted hyena (*Crocuta crocuta*). *Philosophical Transactions of the Royal Society of London, Series B: Biological Sciences* 2007;**362**:523–38. <https://doi.org/10.1098/rstb.2006.1993>

Howell FC, García N. Carnivora (Mammalia) from Lemudong'o (Late Miocene: Narok District, Kenya). *Kirtlandia* 2007;**56**:121–39.

Hürzeler J. Die Lutrinen (Carnivora, Mammalia) aus dem 'Grosseto- Lignit' der Toscana. *Neues Jahrbuch für Geologie und Paläontologie* 1987;**110**:27–48.

Hürzeler J, Engesser B. Les faunes de mammifères néogènes du Bassin de Baccinello (Grosseto, Italie). *Comptes Rendus de l'Academie des Sciences de Paris* 1976;**283**:333–6.

Huxley TH. On the cranial and dental characters of the Canidae. *Proceedings of the Zoological Society of London* 1880;**48**:238–88. <https://doi.org/10.1111/j.1469-7998.1880.tb06558.x>

Iannucci A. The occurrence of suids in the post-olduvai to pre-jaramillo pleistocene of Europe and Implications for late villafranchian biochronology and faunal dynamics. *Quaternary* 2024;**7**:11. <https://doi.org/10.3390/quat7010011>

Iurino DA, Danti M, Della Sala SW *et al.* Modern techniques for ancient bones: vertebrate palaeontology and medical CT analysis [Tecniche moderne per ossa antiche: Paleontologia dei vertebrati e analisi tomografiche mediche]. *Bollettino Della Societa Paleontologica Italiana* 2013;**52**:145–55.

Iurino DA, Mecozzi B, Iannucci A *et al.* A Middle Pleistocene wolf from central Italy provides insights on the first occurrence of *Canis lupus* in Europe. *Scientific Reports* 2022a;**12**:2882. <https://doi.org/10.1038/s41598-022-06812-5>

Iurino DA, Iannucci A, Conti J *et al.* Revised description of the late Miocene *Hyaenictitherium namaquensis* (carnivora, hyaenidae) from As Sahabi (North Africa, Libya). *Historical Biology* 2022b;**34**:1373–80.

Ivanoff DV, Wolsan M, Marciszak A. Brainy stuff of long-gone dogs: a reappraisal of the supposed *Canis* endocranial cast from the Pliocene of Poland. *Naturwissenschaften* 2014;**101**:645–51. <https://doi.org/10.1007/s00114-014-1200-4>

Koepfli KP, Pollinger J, Godinho R *et al.* Genome-wide evidence reveals that African and Eurasian golden jackals are distinct species. *Current Biology: CB* 2015;**25**:2158–65. <https://doi.org/10.1016/j.cub.2015.06.060>

Kostopoulos D, Sen S. Late Pliocene (Villafranchian) mammals from Sirakol Tepe, Ankara, Turkey. *Mitteilungen der Bayerischen Staatssammlung für Paläontologie und historische Geologie* 1999;**39**:165–202.

Kotsakis T, Barisone G, Rook L. Mammalian biochronology in an insular domain: the Italian Tertiary faunas. *Mémoires et Travaux de l'Institut de Montpellier de l'École Pratique des Hautes Études* 1997;**21**:431–41.

Koufos GD. The fossil record of canids (Mammalia: Carnivora: Canidae) in Greece. In: Vlachos E (ed.), *Fossil Vertebrates of Greece Vol. 2: Laurasiatherians, Artiodactyles, Perissodactyles, Carnivorans, and Island Endemics*. Switzerland: Springer Nature, 2022, 577–94.

Kretzoi M. *Kochitis centenii* n.g.n. sp., ein altertümlicher Creodonte aus dem Oberoligozan Siebenburgens. *Földtani Közlöny* 1943;**52**:10–195.

Leidy J. *Notice of Remains of Extinct Vertebrata, from the Valley of the Niobrara River*. Philadelphia: Merrihew & Thompson, 1858.

Lindblad-Toh K, Wade CM, Mikkelsen TS *et al.* Genome sequence, comparative analysis and haplotype structure of the domestic dog. *Nature* 2005;**438**:803–19. <https://doi.org/10.1038/nature04338>

Linnaeus C. *Systema Naturae per Regna Tria Naturae, Secumdem Classes, Ordines, Genera, Species, Cum Characteribus, Differentiis, Synonymis, Locis*. Stockholm: L. Salvius, 1758.

Lund PW. Blik paa Brasiliens dyreverden för sidste Jordomvæltning. *Det Kongelige Danske Videnskabernes Selskabs Naturvidenskabelige og Mathematiske Afhandlinger* 1842;**9**:137–208.

Lyras GA. The evolution of the brain in Canidae (Mammalia: Carnivora). *Scripta Geologica* 2009;**139**:1–39.

Lyras GA, Van Der Geer AAE, Dermitzakis M. Evolution of the brain of Plio/Pleistocene wolves. *Cranium* 2001;**18**:30–40.

Mahdy MA, Zayed M. Computed tomography and cross-sectional anatomy of the head in the red fox (*Vulpes vulpes*). *Anatomia, Histologia, Embryologia* 2020;**49**:708–17.

Marra AC, Solounias N, Carone G *et al.* Palaeogeographic significance of the giraffid remains (Mammalia, Artiodactyla) from Cessaniti (Late Miocene, Southern Italy). L'importance paléogéographique des girafes de Cessaniti (Miocène Supérieur Italie du sud). *Geobios* 2011;**44**:189–97. <https://doi.org/10.1016/j.geobios.2010.11.005>

Martin R. Trois nouvelles espèces de caninae (Canidae, Carnivora) des gisements Plio-Villafranchiens d'Europe. *Documents du Laboratoire de Géologie de la Faculté de Sciences de Lyon* 1973;**57**:87–96.

Meneghini G. Descrizione dei resti di due fiere trovati nelle ligniti mioceniche di Montebamboli. *Atti della Società Italiana di Scienze Naturali* 1862;**4**:17–33.

Merriam JC. Tertiary mammal beds of virgin valley and thousand creeks in Northwestern Nevada, Part II, University of California Publications. *Bulletin of the Department of Geology* 1911;**6**:199–304.

Miller WE, Carranza-Castañeda O. Late Tertiary canids from central Mexico. *Journal of Paleontology* 1998;**72**:546–56. <https://doi.org/10.1017/s002233600002432x>

Montoya P, Morales J, Abella J. *Eucyon debonisi* n. sp., a new Canidae (Mammalia, Carnivora) from the latest Miocene of Venta del Moro (Valencia, Spain). *Geodiversitas* 2009;**31**:709–22. <https://doi.org/10.5252/g2009n4a709>

Morales J, Pickford M, Soria D. Carnivores from the late Miocene and basal Pliocene of the Tugen Hills, Kenya. *Revista de la Sociedad Geológica de España* 2005;**18**:39–61.

Nelson EW, Goldman EA. List of the pumas, with three described as new. *Journal of Mammalogy* 1929;**10**:345–50. <https://doi.org/10.2307/1374125>

Odintzov IA. New species of Pliocene Carnivora, *Vulpes odessana* sp. nov. from the Karst Cave of Odessa. *Paleontologicheskyy Sbornik, Lvov University* 1967;**4**:130–7.

Pandolfi L, Rook L. An enigmatic giraffid from the latest Miocene of Italy: taxonomy, affinity, and paleobiogeographic implications. *Journal of Mammalian Evolution* 2023;**30**:403–13. <https://doi.org/10.1007/s10914-023-09654-8>

Pandolfi L, Marra AC, Carone G *et al.* A new rhinocerotid (Mammalia, Rhinocerotidae) from the latest Miocene of Southern Italy. *Historical Biology* 2021;**33**:194–208. <https://doi.org/10.1080/08912963.2019.1602615>

Papstein K, Steiner M, Aerni M. *ZBrush Characters and Creatures*. Worcester: 3DTotal Publishing, 2015.

Patacca E, Scandone P, Carnevale G. The Miocene vertebrate-bearing deposits of Scontrone (Abruzzo, Central Italy): stratigraphic and paleoenvironmental analysis. *Geobios* 2013;**46**:5–23. <https://doi.org/10.1016/j.geobios.2012.11.001>

Paulli S. Über die Pneumaticität des Schädels bei den Säugethieren. III. Über die Morphologie des Siebbeins und Pneumaticität bei den Insectivoren, Hyracoideen, Chiropteren, Carnivoren, Pinnipeden, Edentaten, Rodentien, Prosimien und Primaten. *Journal of Morphology* 1900;**28**:483–564.

Pellegrino L, Abe K, Gennari R *et al.* An integrated micropaleontological study of the diatomaceous deposits of the Monferrato Arc (Piedmont Basin, NW Italy) provides new insights into the Messinian paleoceanographic evolution of the northernmost Mediterranean region. *Marine Micropaleontology* 2020a;**160**:101910. <https://doi.org/10.1016/j.marmicro.2020.101910> Pellegrino L, Dela Pierre F, Jordan RW *et al.* The upper Miocene diatomaceous sediments of the northernmost Mediterranean region: a lamina-scale investigation of an overlooked paleoceanographic archive. *Sedimentology* 2020b;**67**:3389–421. <https://doi.org/10.1111/sed.12748>

Perini FA, Russo CAM, Schrago CG. The evolution of South American endemic canids: a history of rapid diversification and morphological parallelism. *Journal of Evolutionary Biology* 2010;**23**:311–22. <https://doi.org/10.1111/j.1420-9101.2009.01901.x>

Perri AR, Mitchell KJ, Mouton A *et al.* Dire wolves were the last of an ancient New World canid lineage. *Nature* 2021;**591**:87–91. <https://doi.org/10.1038/s41586-020-03082-x>

Peters N, Rook L, de Vos J. *Eucyon* sp. (Mammalia, Carnivora, Canidae, Caninae), an early dog from Mill-Langenboom, The Netherlands. *Cainozoic Research* 2015;**15**:55–8.

Petrocchi M, Consalvi E. La restaurazione, il cardinale Consalvi e la riforma del 1816. *Studi e Documenti di Storia del Risorgimento* 1941;**22**:1.

Pilgrim GE. Presidential address to the geological section of the 12th Indian Science congress. *Proceedings of the 12th Indian Scientific Congress* 1925:200–18.

Piñero P, Agustí J, Oms O *et al.* Early Pliocene continental vertebrate Fauna at Puerto de la Cadena (SE Spain) and its bearing on the marine-continental correlation of the Late Neogene of Eastern Betics. *Palaeogeography, Palaeoclimatology, Palaeoecology* 2017;**479**:102–14. <https://doi.org/10.1016/j.palaeo.2017.04.020>

Pons-Moyà J, Crusafont M. El *Canis cipio* Crusafont (1978), comparación con los cánidos del Plioceno y Pleistoceno europeo. *Acta Geológica Hispánica* 1978;**13**:133–6.

Pons-Moya J, Crusafont-Pairò M. Sobre la identidad del «*Canis*» *adoxus* Martin (1973) y su implicación en el conocimiento del género *Vulpes*. *Acta Geologica Hispanica* 1978;**4**:129–32.

Prevosti FJ. Phylogeny of the large extinct South American canids (Mammalia, Carnivora, Canidae) using a ‘total evidence’ approach. *Cladistics* 2010;**26**:456–81. <https://doi.org/10.1111/j.1096-0031.2009.00298.x>

Radinsky LB. Outlines of canid and felid brain evolution. *Annals of the New York Academy of Sciences* 1969;**167**:277–88. <https://doi.org/10.1111/j.1749-6632.1969.tb20450.x>

Radulescu C, Samson PM, Petculescu A *et al.* Pliocene large mammals of Romania grandes mamíferos del plioceno de Rumania. *Coloquios de Paleontología* 2003;**1**:549–58.

Rook L. '*Canis*' *monticiniensis* sp. nov., a new Canidae (Carnivora, Mammalia) from the late Messinian of Italy. *Bollettino della Società Paleontologica Italiana* 1992;**31**:151–6.

Rook L. *I Cani dell'Eurasia dal Miocene Superiore al Pleistocene Medio*. Unpublished Ph.D. Thesis, Universities of Modena, Bologna, Firenze and Roma 'La Sapienza', 1993.

Rook L. Late Turolian *Mesopithecus* (Mammalia, Primates, Colobinae) from Italy. *Journal of Human Evolution* 1999;**36**:535–47. <https://doi.org/10.1006/jhev.1998.0288>

Rook L. The wide ranging genus *Eucyon* Tedford & Qiu, 1996 (Mammalia, Carnivora, Canidae, Canini) in the Mio-Pliocene of the Old World. *Geodiversitas* 2009;**31**:723–41. <https://doi.org/10.5252/g2009n4a723>

Rook L. *La Fauna Messiniana di Cava Monticino (Brisighella, RA)*. Memorie dell'Istituto Italiano di Speleologia Serie II-Vol. 37, 2021 Società Speleologica Italiana: Bologna.

Rook L, Abbazzi L, Engesser B. An overview on the Italian Miocene land mammal faunas. In: Agustí J, Rook L, Andrews P (eds), *The Evolution of Neogene Terrestrial Ecosystems in Europe*. Cambridge: Cambridge University Press, 1999;191–204.

Rook L, Gallai G, Torre D. Lands and endemic mammals in the Late Miocene of Italy: constraints for paleogeographic outlines of Tyrrhenian area. *Palaeogeography, Palaeoclimatology, Palaeoecology* 2006;**238**:263–9. <https://doi.org/10.1016/j.palaeo.2006.03.027>

Rook L, Bartolini-Lucenti S, Bukhsianidze M *et al.* The Kvabebi Canidae record revisited (late Pliocene, Sighnaghi, eastern Georgia). *Journal of Paleontology* 2017;**91**:1258–71.

Rüppell E. *Neue Wirbelthiere zu der Fauna von Abyssinien Gehörig*. Frankfurt am Main: Siegmund Schmerber, 1840.

Sakai ST, Arsznov BM, Lundrigan BL *et al.* Brain size and social complexity: a computed tomography study in hyaenidae. *Brain Behavior and Evolution* 2011;**77**:91–104. <https://doi.org/10.1159/000323849>

Sami M. *Il Parco Museo Geologico Cava Monticino, Brisighella: una Guida e una Storia, Regione Emilia-Romagna e Provincia di Ravenna*. Faenza: Tipografia Carta Bianca, 2007.

Sardella R. Remarks on the Messinian carnivores (Mammalia) of Italy. *Bollettino della Società Paleontologica Italiana* 2008;**47**:195–202.

Sardella R, Bertè D, Iurino DA *et al.* The wolf from Grotta Romanelli (Apulia, Italy) and its implications in the evolutionary history of *Canis lupus* in the Late Pleistocene of Southern Italy. *Quaternary International* 2014;**328-329**:179–95.  
<https://doi.org/10.1016/j.quaint.2013.11.016>

Say T. *Canis latrans*. In: Carey HC, Lea I (ed.), *Account of an Expedition from Pittsburgh to the Rocky Mountains*. Philadelphia: Philadelphia editorial, 1823.

Schinz HR. *Vulpes rueppellii*. In: Cuvier's Thierreich G, (ed). *Das Thierreich Eingetheilt Nach dem bau der Thiere als Grundlage Iher Naturgeschichte und der Vergleichenden Anatomie*. Stuttgart & Tübingen: J.G. Cotta'schen Buchhandlung, 1825; Vol. 4.

Schreber JCD. *Die Säugthiere in Abbildungen Nach der Natur mit Beschreibungen* (Erster Theil). Erlangen: Verlag Wolfgang Walther, 1775.

Seguenza L. I vertebrati fossili della provincia di Messina: Parte II. Mammiferi e geologia del piano Pontico. *Bollettino Della Società Geologica Italiana* 1902;**21**:115–72.

Seguenza L. Nuovi resti di mammiferi fossili di Gravitelli presso Messina. *Bollettino Della Società Geologica Italiana* 1907;**26**:7–119.

Shaw G. *General Zoology or Systematic Natural History*. London: G. Kearsley, 1800.

Simpson GG. Large Pleistocene felines of North America. *American Museum Novitates* 1941;**1136**:1–27.

Simpson GG, Roe A, Lewontin RC. *Quantitative Zoology*. NY: Harcourt Brace, 1960.

Sotnikova MV. The carnivore mammals from the Pliocene to the Early Pleistocene. *Stratigraphic Significance Moscow: Nauka*, 1989 [in Russian].

Sotnikova M, Rook L. Dispersal of the Canini (Mammalia, Canidae: Caninae) across Eurasia during the Late Miocene to Early Pleistocene. *Quaternary International* 2010;**212**:86–97. <https://doi.org/10.1016/j.quaint.2009.06.008>

Spassov N, Rook L. *Eucyon marinae* sp. nov. (Mammalia, Carnivora), a new canid species from the Pliocene of Mongolia, with a review of forms referable to the genus. *Rivista Italiana di Paleontologia e Stratigrafia* 2006;**112**:123–33.

Sundevall CJ. Nya Mammalia från Sydafrika. *Öfversigt af Kongl Svenska Vetenskaps-Akademiens Förhandlingar Stockholm* 1847;**3**:118–21.

Tedford RH, Qiu Z-X. A new canid genus from the Pliocene of Yushe, Shanxi Province. *Vertebrata Palasiatica* 1996;**34**:27–40.

Tedford RH, Wang X-M, Taylor BE. Phylogenetic systematic of the North American fossil Caninae (Carnivora: Canidae). *Bulletin of the American Museum of Natural History* 2009;**325**:1–218. <https://doi.org/10.1206/574.1>

Teilhard de Chardin P, Piveteau J. Les mammifères fossiles de Nihowan (Chine). *Annales de Paléontologie* 1930;**19**:1–134.

Temminck C. Sur le genre hyena, et description d'une espece nouvelle, decouverte en Afrique. *Annales generals des sciences physiques, Bruxelles De l'impr. De Weissenbruch* 1820;**3**:46–57.

Torre D, Abbazzi L, Delfino M, *et al.* Mammal palaeobioprovinces in the Italian Miocene. *XIth RCMNS Congress 2000. Abstract book, Fez, Morocco*: **43**.

Valenciano A, Morales J, Govender R. *Eucyon khoikhoi* sp. nov. (Carnivora: Canidae) from Langebaanweg 'E' Quarry (early Pliocene, South Africa): the most complete African canini from the Mio-Pliocene. *Zoological Journal of the Linnean Society* 2022;**194**:366–94.

Van Valkenburgh B, Pang B, Bird D *et al.* Respiratory and olfactory turbinals in feliform and caniform carnivorans: the influence of snout length. *Anatomical Record (Hoboken, N.J.: 2007)* 2014;**297**:2065–79. <https://doi.org/10.1002/ar.23026>

Villa A, Carnevale G, Pavia M *et al.* An overview of the late Miocene vertebrates from the fissure fillings of Monticino Quarry (Brisighella, Italy), with new data on non-mammalian taxa. *Rivista Italiana di Paleontologia e Stratigrafia* 2022;**127**:297–354.

Vinuesa V, Iurino DA, Durell-Malapeira J *et al.* Inferences of social behavior in bone-cracking hyaenids (Carnivora, Hyaenidae) based on digital paleoneurological techniques: implications for human–carnivoran interactions in the Pleistocene. *Quaternary International* 2016;**413**:7–14. <https://doi.org/10.1016/j.quaint.2015.10.037>

Viranta S, Atickem A, Werdelin L *et al.* Rediscovering a forgotten canid species. *BMC Zoology* 2017;**2**:1–9.

Van Valkenburgh B. Skeletal and dental predictors of body mass in carnivores. In: Damuth J, MacFadden BJ (eds), *Body Size in Mammalian Paleobiology: Estimation and Biological Implications*. Cambridge: Cambridge University Press 1990; 181–205.

Von den Driesch A. A guide to the measurement of animal bones from archaeological sites. *Peabody Museum Bulletins* 1976;**1**:1–137.

Wang X-M, Tedford RH, Antón M. *Dogs: Their Fossil Relatives and Evolutionary History*. NY: Columbia University Press, 2008.

Wayne RK, Ostrander EA. Lessons learned from the dog genome. *Trends in Genetics: TIG* 2007;**23**:557–67. <https://doi.org/10.1016/j.tig.2007.08.013>

Weithofer KA. Alcune osservazione sulla fauna delle ligniti di Casteani e di Montebamboli (Toscana). *Bolletino del Reale Comitato Geologico d'Italia* 1888;**19**:363–8.

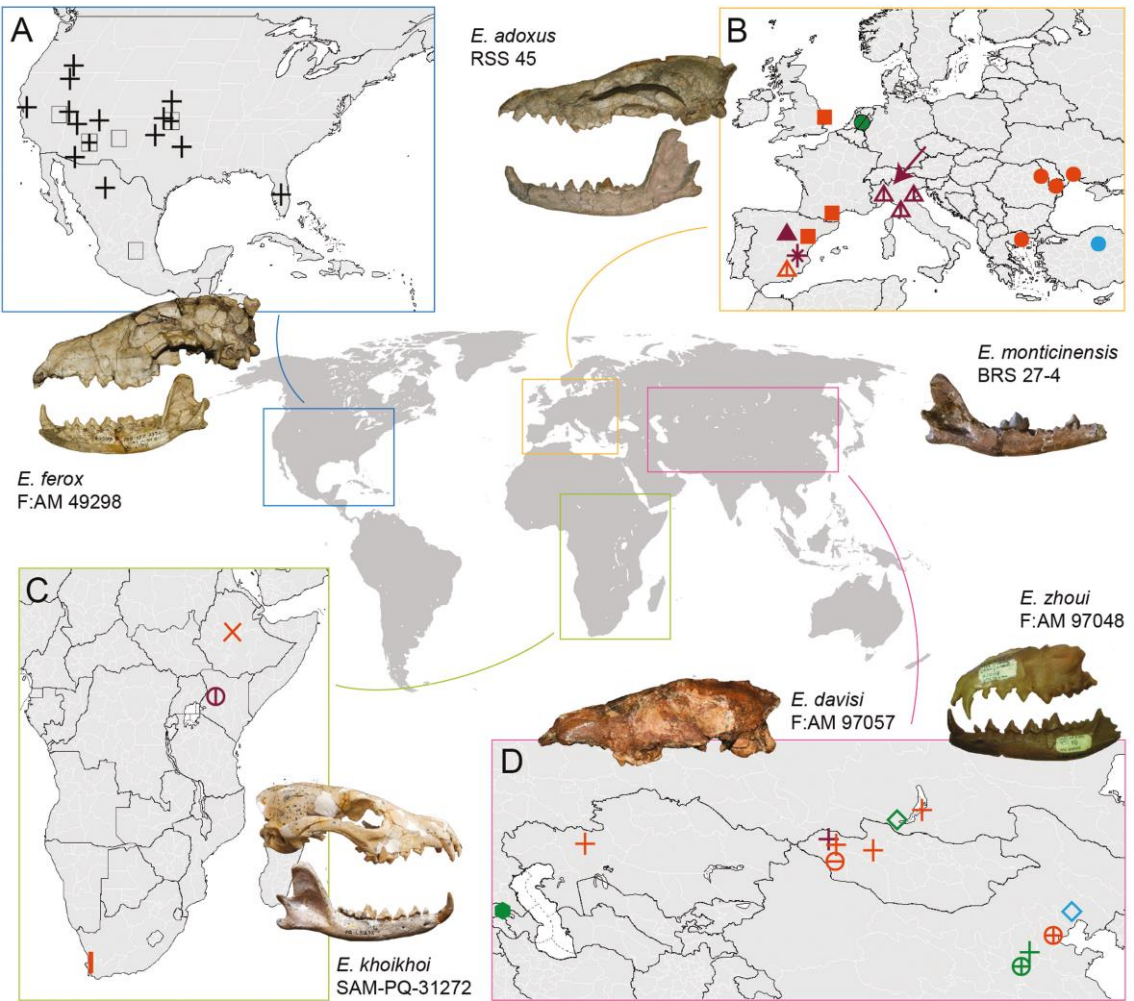
Werdelin L, Dehghani R. Carnivora. In: Harrison T (ed.), *Paleontology and Geology of Laetoli: Human Evolution in Context. Vertebrate Paleobiology and Paleoanthropology Series*. Dordrecht: Springer, 2011;189–232.

Werdelin L, Lewis ME, Haile-Selassie Y. A critical review of African species of *Eucyon* (Mammalia; Carnivora; Canidae), with a new species from the Pliocene of the Woranso-Mille Area, Afar Region, Ethiopia. *Papers in Palaeontology* 2015;**1**:33–40.

Zimmerman EAW. *Geographische Geschichte des Menschen, und der Vierfüßigen Thiere*. Leipzig: Weygandschen Buchhandlung, 1780.

Zrzavý J, Duda P, Robovsky J *et al.* Phylogeny of the Caninae (Carnivora): combining morphology, behaviour, genes and fossils. *Zoologica Scripta* 2018;**47**:373–89.

**Figure 1.** Geographical and chronological distribution of *Eucyon*. The location of Verduno is shown by the arrow in B. Some of the most complete cranial specimens are shown for each geographical area. The image of *Eucyon ferox* is from Bartolini-Lucenti and Rook (2021); the image of *Eucyon khoikhoi* is from Valenciano *et al.* (2021); and the image of *Eucyon zhoui* is from Rook (2009).



- Early/Late Hemphillian**  
 + *E. davisi* □ *E. ferox*
- Late Miocene**  
 + *E. davisi*  
 ▲ *E. cipio*  
 \* *E. debonisi*  
 ⊕ "E." *intrepidus*  
 ▲ *E. monticinensis*
- Early Pliocene**  
 + *E. davisi*  
 ▲ *E. monticinensis*  
 ■ *E. adoxus*  
 ● *E. odessanus*  
 | *E. khoikhoi*  
 ⊖ *E. marinae*  
 × *E. kuta*  
 ⊕ *E. zhoui*
- Late Pliocene**  
 ● *Eucyon* sp. from Mill-Langenboom  
 ● *Eucyon* sp. from Kvabebi  
 + *E. davisi*  
 ⊕ *E. zhoui*  
 ◇ *E. minor*
- Early Pleistocene**  
 ◇ *E. minor* ● *E. odessanus*

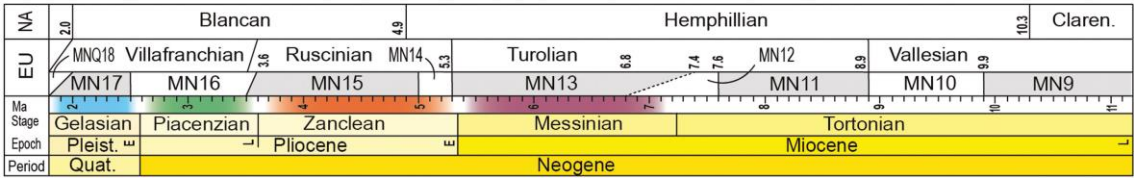


**Figure 2.** Orthomosaic map of the block containing the *Eucyon* skeleton from Verduno before preparation, obtained from a *Structure-from-Motion* photogrammetric model. Scale bar: 50 mm.

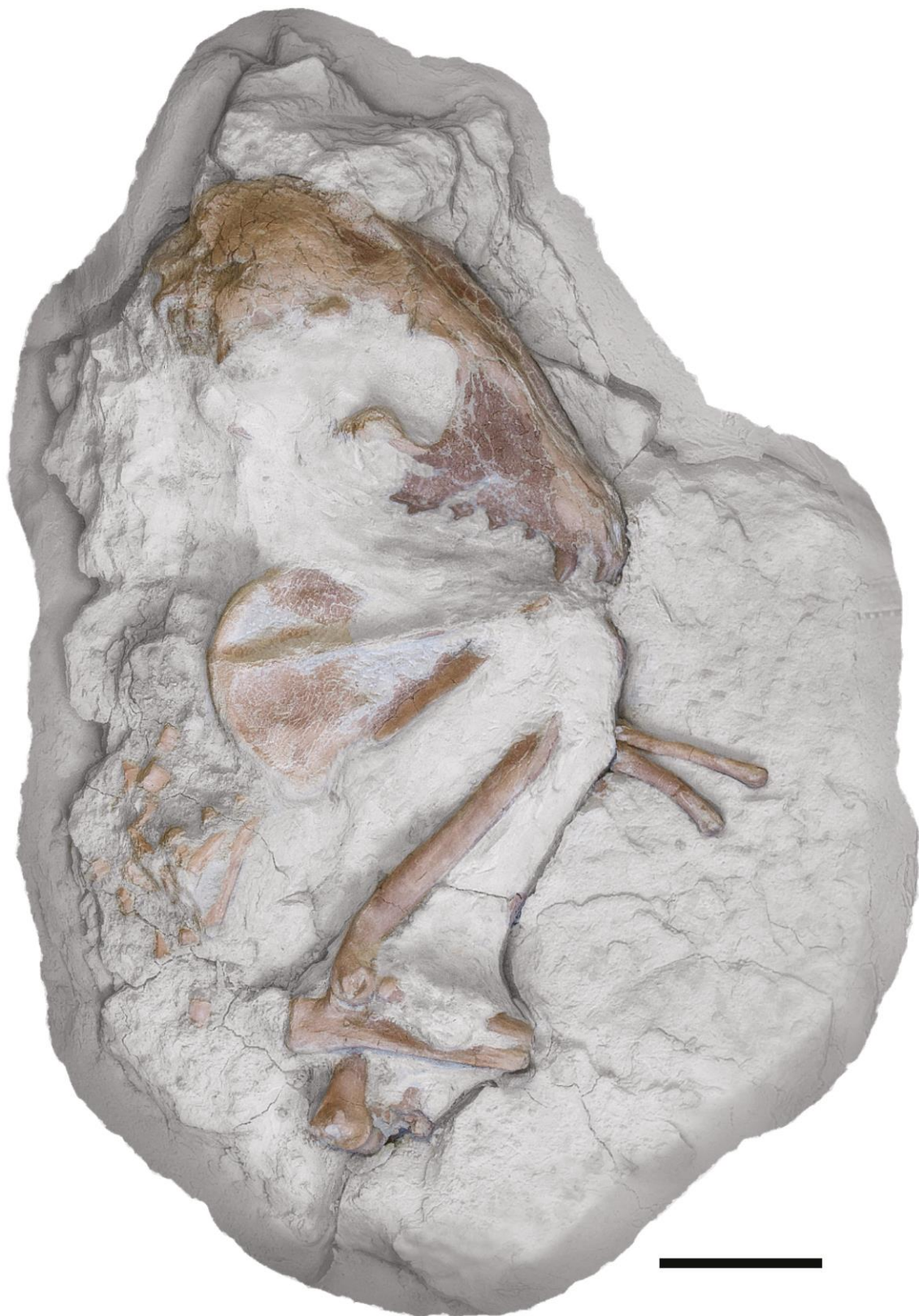


**Figure 3.** Skull and atlas of *Eucyon monticinensis* (MGPT-PU 135418) from Verduno (Italy). Skull in: A, dorsal; B, C, right- and left-lateral; D, ventral; E, posterior views. F, left i2 and i3 in posterior view; G, left c in right-lateral view; H, atlas in dorsal view. Scale bar: 20 mm.

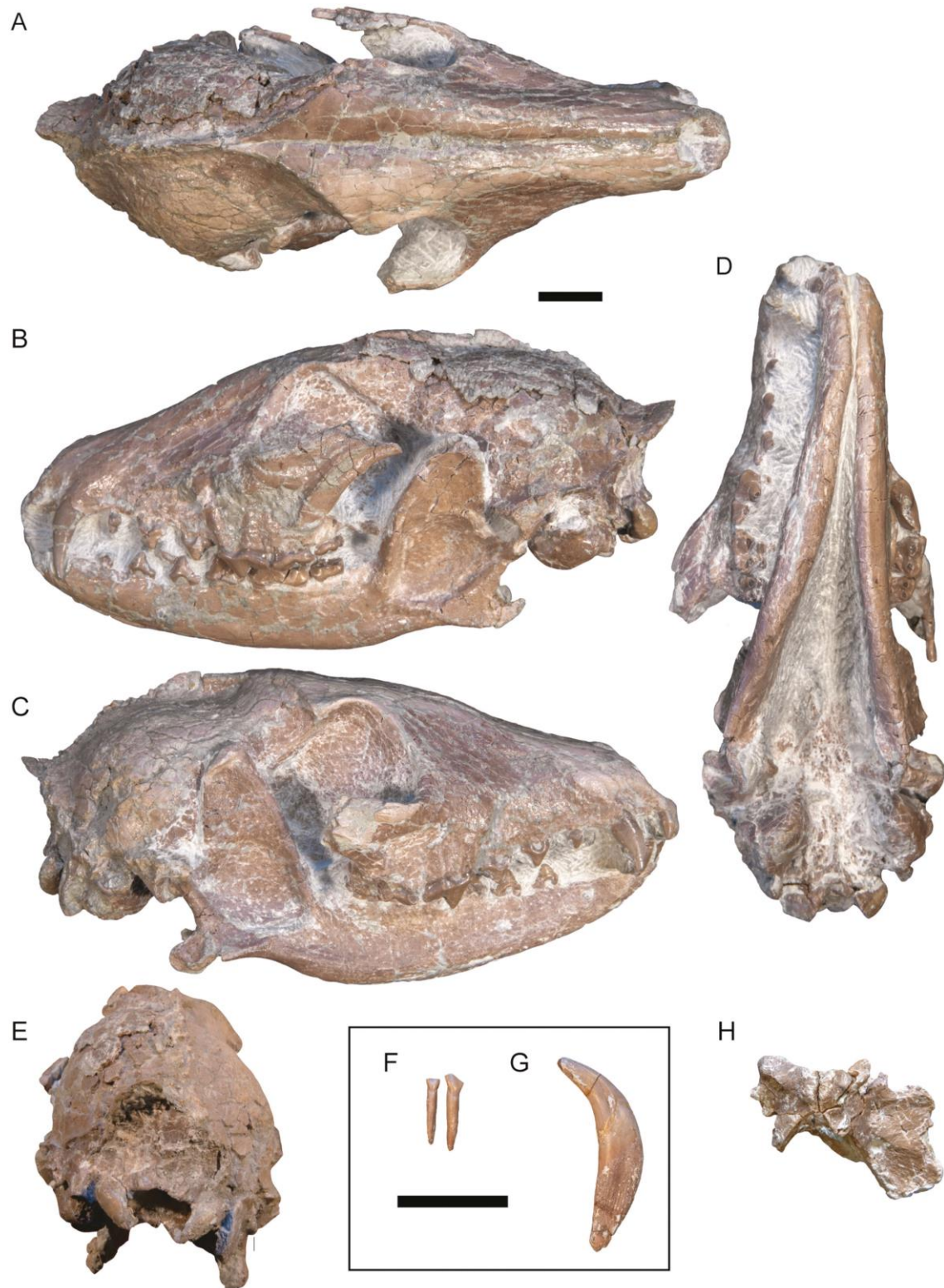


**Figure 4.** Postcranial of *Eucyon monticinensis* (MGPT-PU 135418) from Verduno (Italy). A1, A2, left and right scapulae, cervical (axis, C3–C7) and thoracic (T2–T4) vertebrae in lateral views; B, 5th and 6th thoracic vertebrae (T5, T6) in lateral view; C1, left and right humeri in lateral views; C2, left and right humeri in caudal views; D1, left and right radii in medial views; D2, left and right radii in cranial views; E1, right and left ulnae in medial views; E2, right and left ulnae in cranial views; F, left carpus, metacarpus and phalanges in cranial view; G, sternebra in dorsal view. Scale bar: 20 mm.

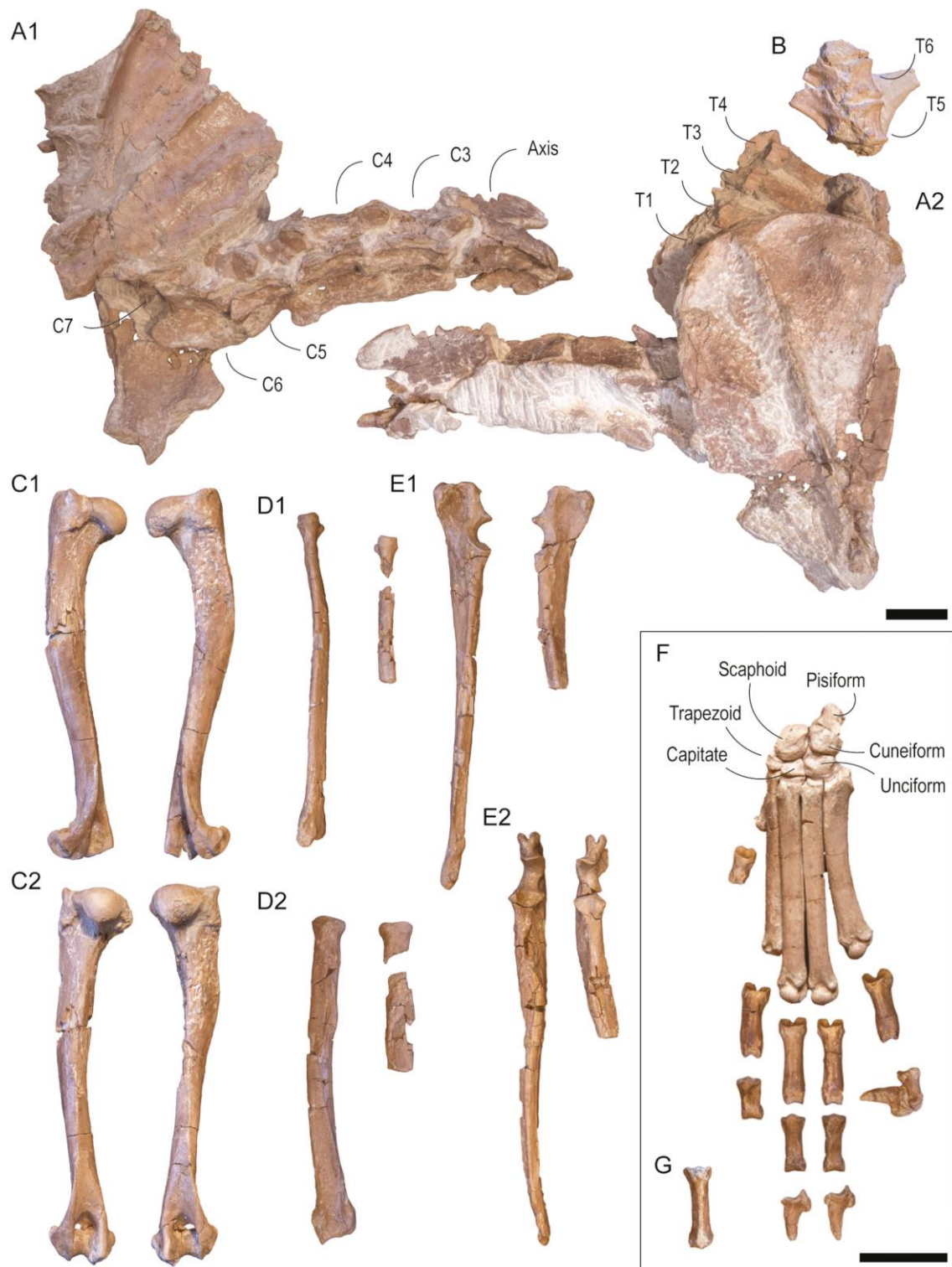


**Figure 5.** Volume rendering of the skull of *Eucyon monticiniensis* MGPT-PU 135418. A, complete skull in left-lateral view; B, separate cranium and mandible in left-lateral view; C, bone tissue in transparency in left-lateral view; D, complete skull in right-lateral view; E, separate cranium and mandible in right-lateral view; F, bone tissue in transparency in right-lateral view; G, H, cranium with bone tissue in transparency in dorsal views; I, J,

skull and cranium in ventral views; K, L, mandible in ventral and occlusal views; M, N, skull and cranium with bone tissue in transparency in rostral views; O, P, skull and cranium with bone tissue in transparency in caudal views; Q, R, mandible in rostral and caudal views. The frontal sinuses are marked in red, the brain in light blue, and the teeth in grey placed above the brain. Scale bar: 50 mm.

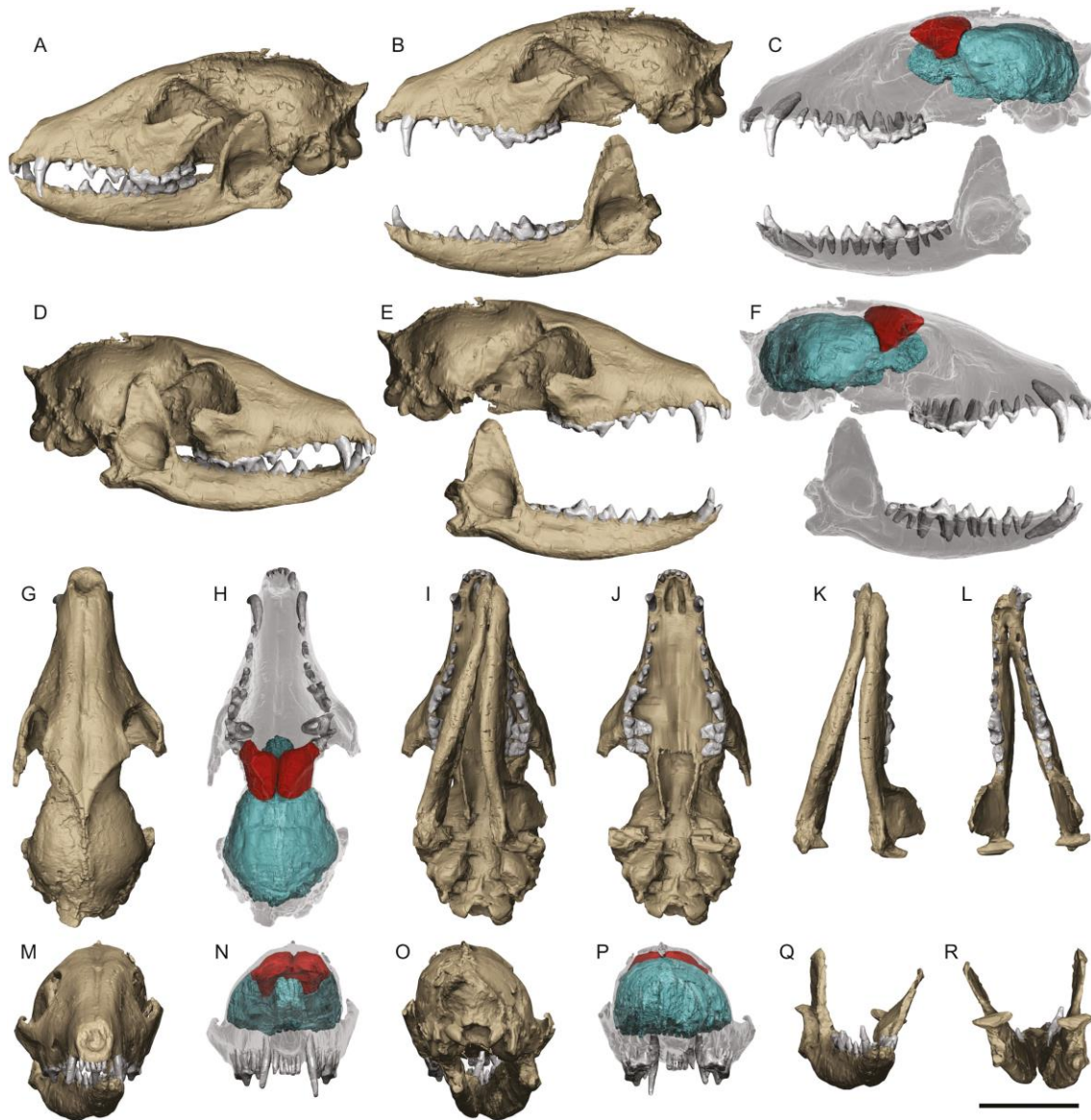


**Figure 6.** Comparison of brain endocasts. Dorsal and left lateral views of: A, *Eucyon monticinensis* MGPT-PU 135418; B, *Eucyon davisi* F:AM 97057; C, *Vulpes vulpes*; D, *Speothos venaticus*; E, *Lupulella mesomelas*; F, *Canis aureus*; G, *Canis latrans*; H, *Canis*

*simensis*; I, *Canis lupus italicus*; J, *Lycaon pictus*. Abbreviations: cs, coronal sulcus; cg, coronal gyrus; ecg, ectolateral gyrus; eg, ectosylvian gyrus; eng, endolateral gyrus; es, ectolateral sulcus; lf, longitudinal fissure; ls, lateral sulcus; ob, olfactory bulb; og, orbital gyrus; op, olfactory peduncle; pg, prorean gyrus; ps, precruciate sulcus; rf, rhinal fissure; sg, sigmoid gyrus; ssg, suprasylvian gyrus; ss, suprasylvian sulcus. The arrows facing downwards indicate a flat frontal cortex, while those facing upwards show the dorsal expansion of the cortex. All the images are normalised.

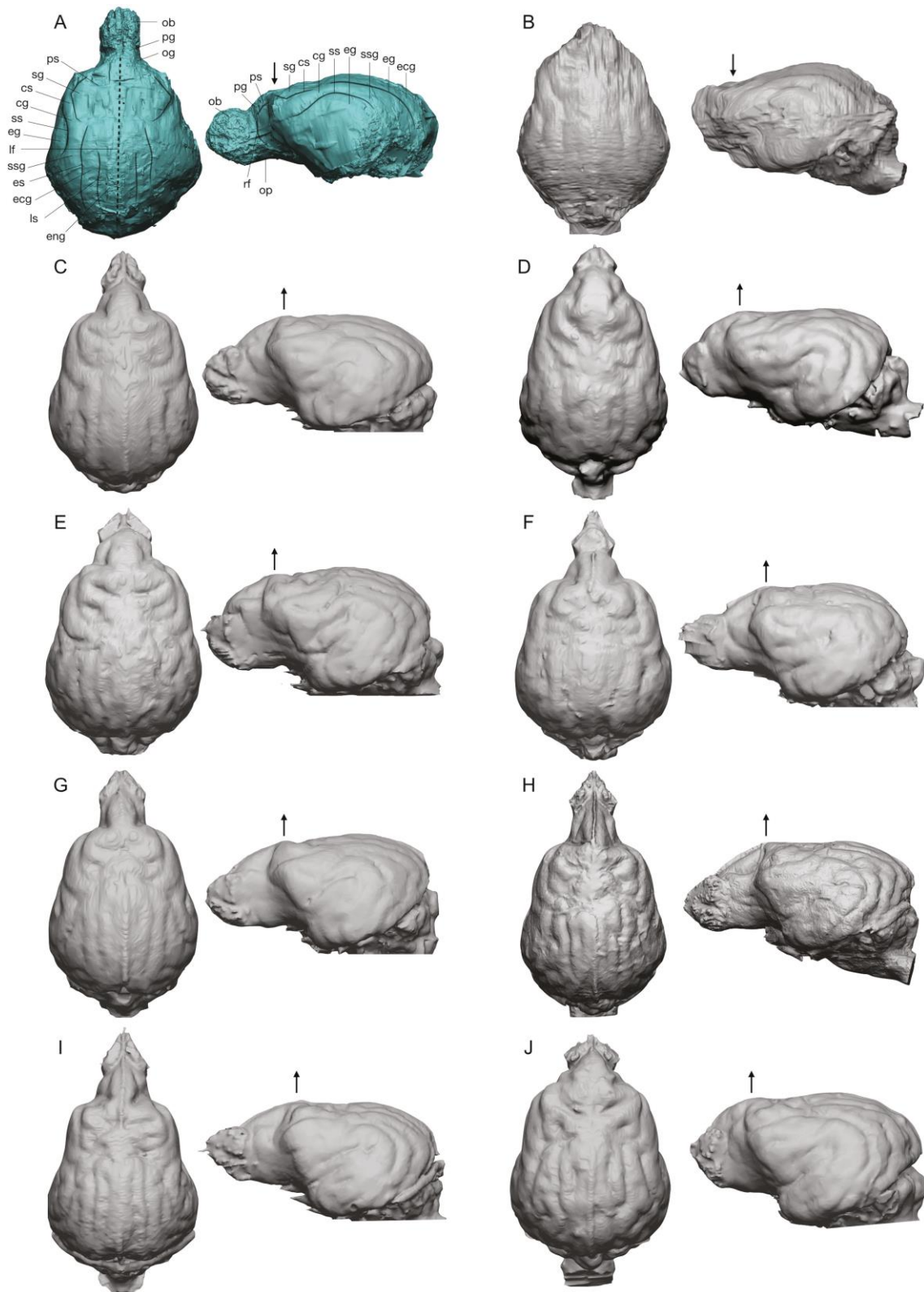


**Figure 7.** *Eucyon monticinensis* MGPT-PU 135418. Volume rendering of: A, upper; B, lower teeth. From top right to bottom right, the buccal and lingual sides of the following tooth rows are shown in order: upper right, upper left, lower left, and lower right. Line

drawings of left P4– M2 and right p4–m2 in occlusal views are also shown. Scale bar: 20 mm.



**Figure 8.** Comparative drawings of the few available skulls of *Eucyon* from different localities, in lateral (1) and dorsal (2) views. From top left: A, MGPT-PU 135418 from Verduno; B, *Eucyon davisii* based on cranium (F:AM 63007, F:AM 63009, F:AM 63038, F:AM 63058) and mandible (F:AM 63009B, F:AM 63038, F:AM 63058) from Arizona and *Eucyon davisii* based on cranium (F:AM 97056, F:AM 97057) from the Yushe Basin; C, *Eucyon zhoui* V12181 (THP 10199) from the Yushe Basin [holotype; mirrored from Tedford and Qiu (1996)]; D, *Eucyon adoxus* NMB Rss.45 from St. Estève (holotype); E, *Eucyon ferox* F:AM 49298 from Nevada [from Bartolini-Lucenti and Rook (2021)]; F, *Eucyon khoikhoi* SAM-PQL-31272 from Langebaanweg (holotype; from Valenciano *et al.*, 2021). Not in scale. Artwork by L. Sorbelli.

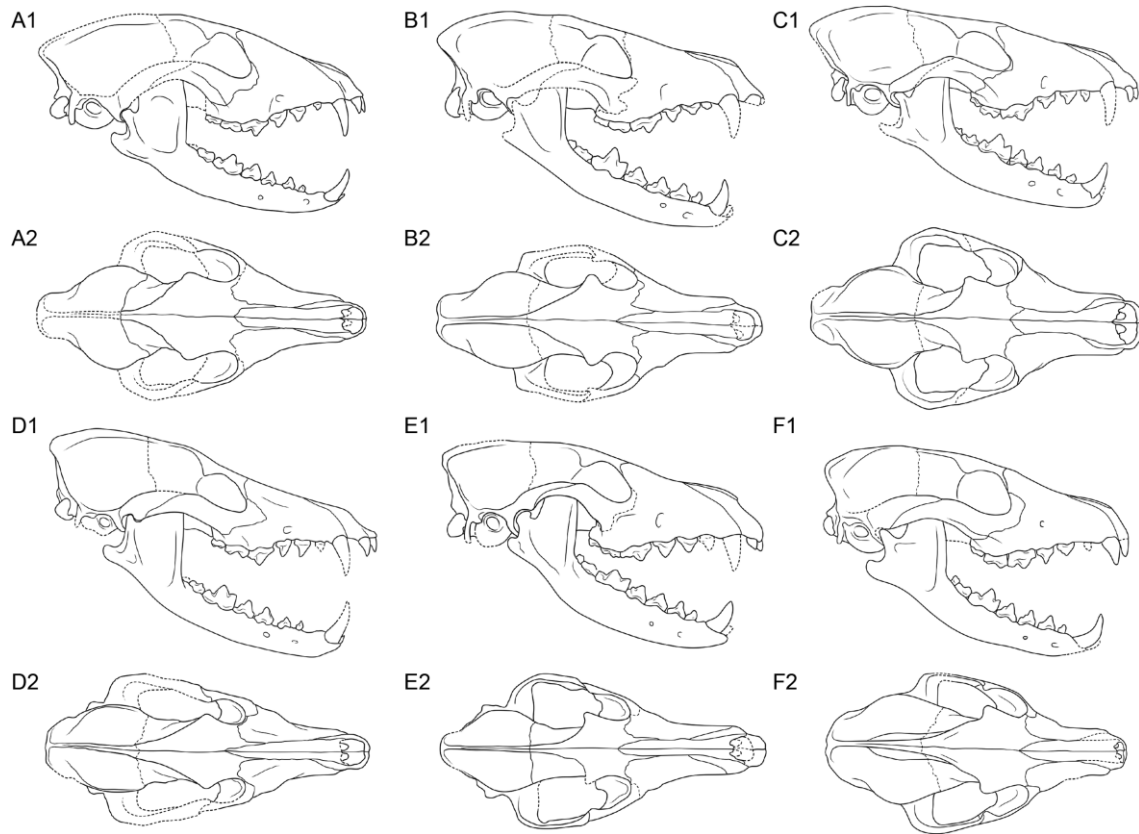
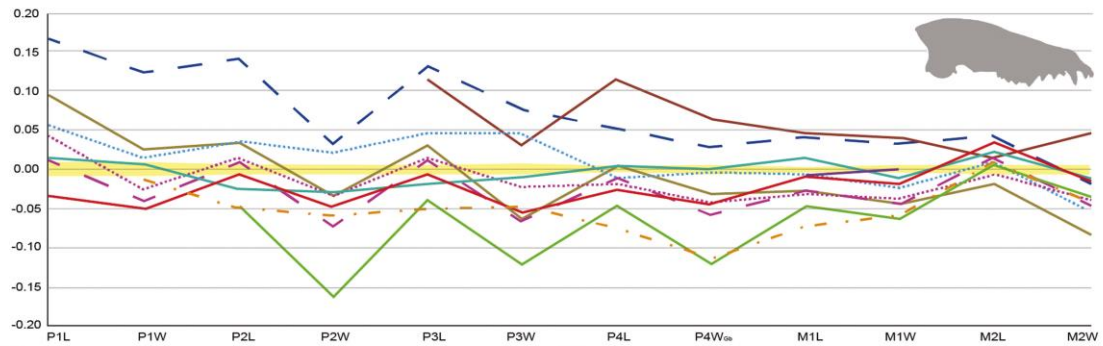


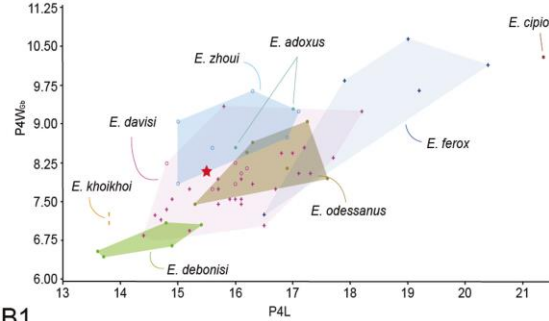
**Figure 9.** Log10 ratio diagrams (A1, B1) and bivariate plots (A2, A3, B2, B3) showing the relationships between selected dental measurements in MGPT-PU 135418 from Verduno and numerous *Eucyon* samples. The extant *Canis aureus* is used as the reference baseline in log10 ratio diagrams; the bars are  $\pm 1\sigma$  for the individuals used to typify the

standard. Abbreviation: A, Asia; NA, North America. All raw data are reported in Supporting Information, Tables S6–S8.

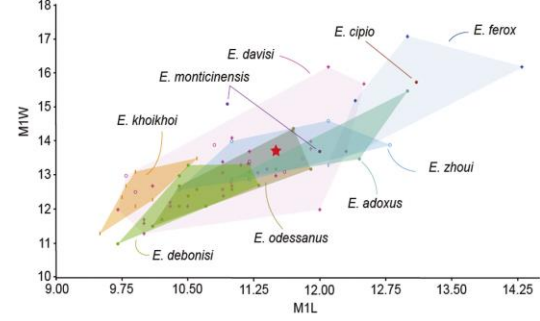
A1



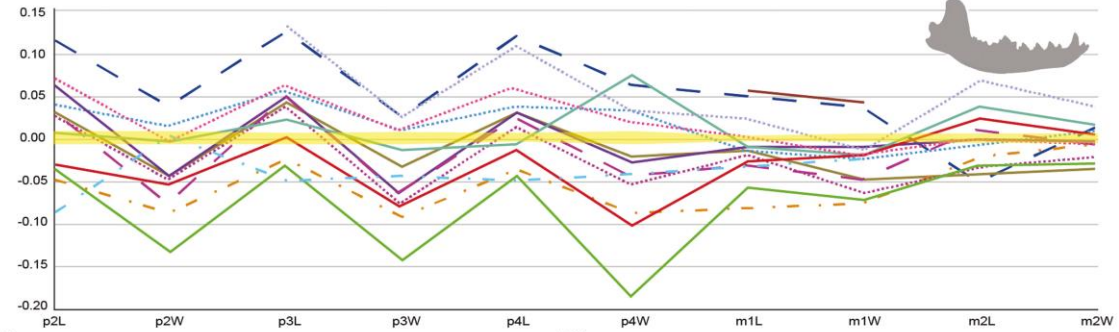
A2



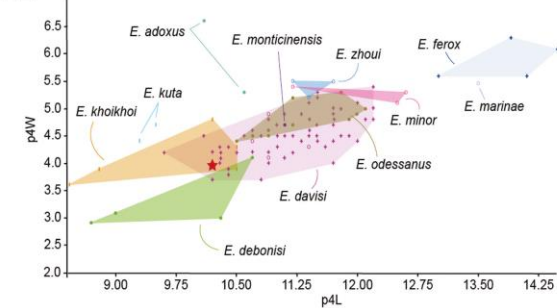
A3



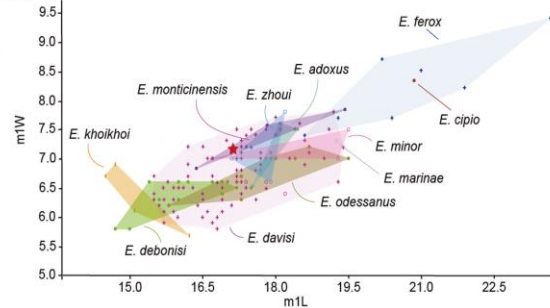
B1



B2



B3



- - or + *Eucyon* from North America    - - *E. ferox*    ..... *E. marinae*    - - *E. adoxus*    - - *Eucyon* from Verduno ★  
 ..... or o *Eucyon* from Asia    - - *E. davis* NA    ..... *E. minor*    - - *E. debonisi*    - - *E. khoikhoi*  
 - - or • *Eucyon* from Europa    ..... *E. davis* A    - - *E. cipio*    - - *E. monticinis*    - - *E. kuta*  
 - - or | *Eucyon* from Africa    ..... *E. zhoui*    - - *E. odessanus*    - - *C. aureus*

**Figure 10.** CT-based comparison of crania, frontal sinuses and brain endocasts of a selected sample of fossil and extant canids. Dorsal and left lateral views of: A, *Eucyon monticinensis* MGPT-PU 135418; B, *Eucyon davisi* F:AM 97057; C, *Eucyon adoxus* NMB Rss.45; D, *Vulpes vulpes*; E, *Vulpes lagopus*; F, *Speothos venaticus*; G, *Lupulella mesomelas*; H, *Lupulella adusta*; I, *Canis aureus*; J, *Canis lupaster*; K, *Canis latrans*; L, *Canis simensis*; M, *Canis etruscus*; N, *Canis arnensis*; O, *Canis lupus*; P, *Canis lupus* from Grotta Romanelli; Q, *Canis lupus italicus*; R, *Canis lupus lycaon*; S, *Canis lupus baileyi*; T, *Lycaon pictus*. Frontal sinuses are marked in red, the brain in light blue. Images B, C, E, H, J are modified from Frosali *et al.* (2023). Scale bar: 50 mm.

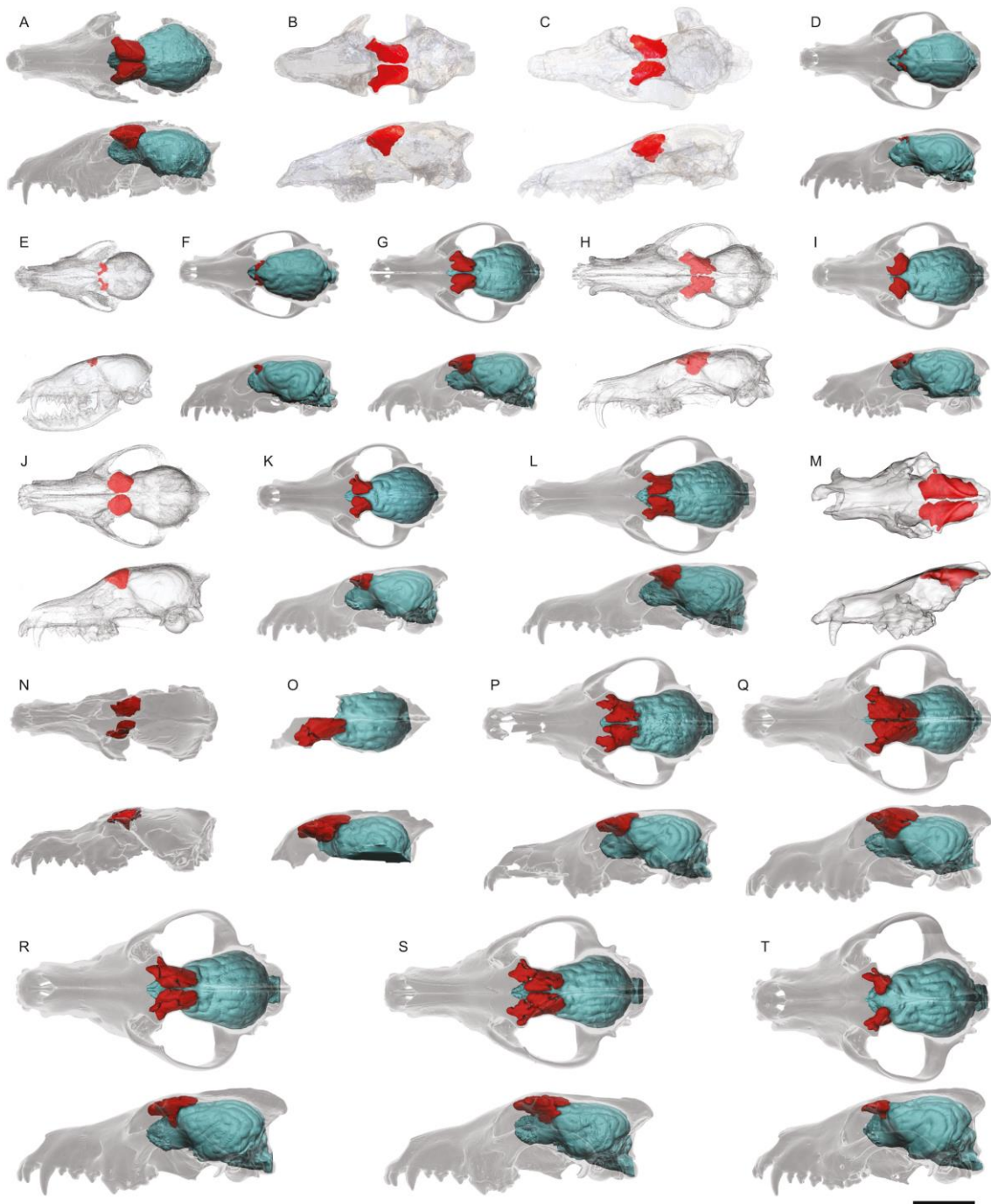


**Figure 11.** Strict consensus tree showing the phylogenetic relationships between extant and extinct (†) Canidae. Node numbers are indicated. The systematics of *Eucyon khoikhoi* and *Eucyon ferox* are dubitable. The paraphyletic Vulpini are indicated by a dashed line due to their uncertain systematic status (see main text).

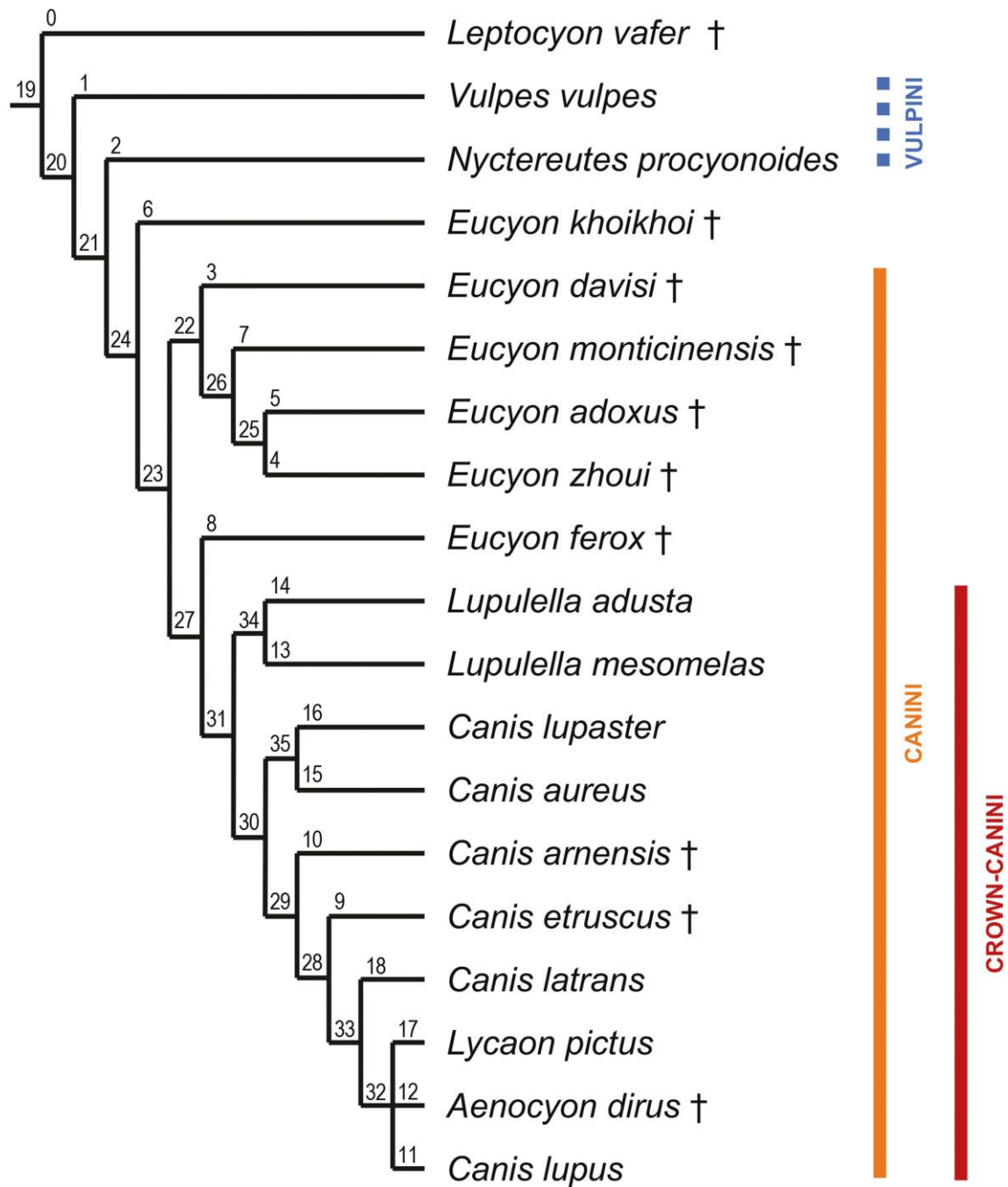


**Figure 12.** Reconstruction of *Eucyon monticiniensis* based on the specimen MGPT-PU 135418. Virtually articulated skeleton in: A, left; B, right; C, rostral; D, caudal; E, dorsal; E, ventral views; G, step-by-step reconstruction from the articulated skeleton to the life appearance of the specimen. The missing parts marked in blue were obtained by mirroring the preserved bones. Artwork by D.A. Iurino.

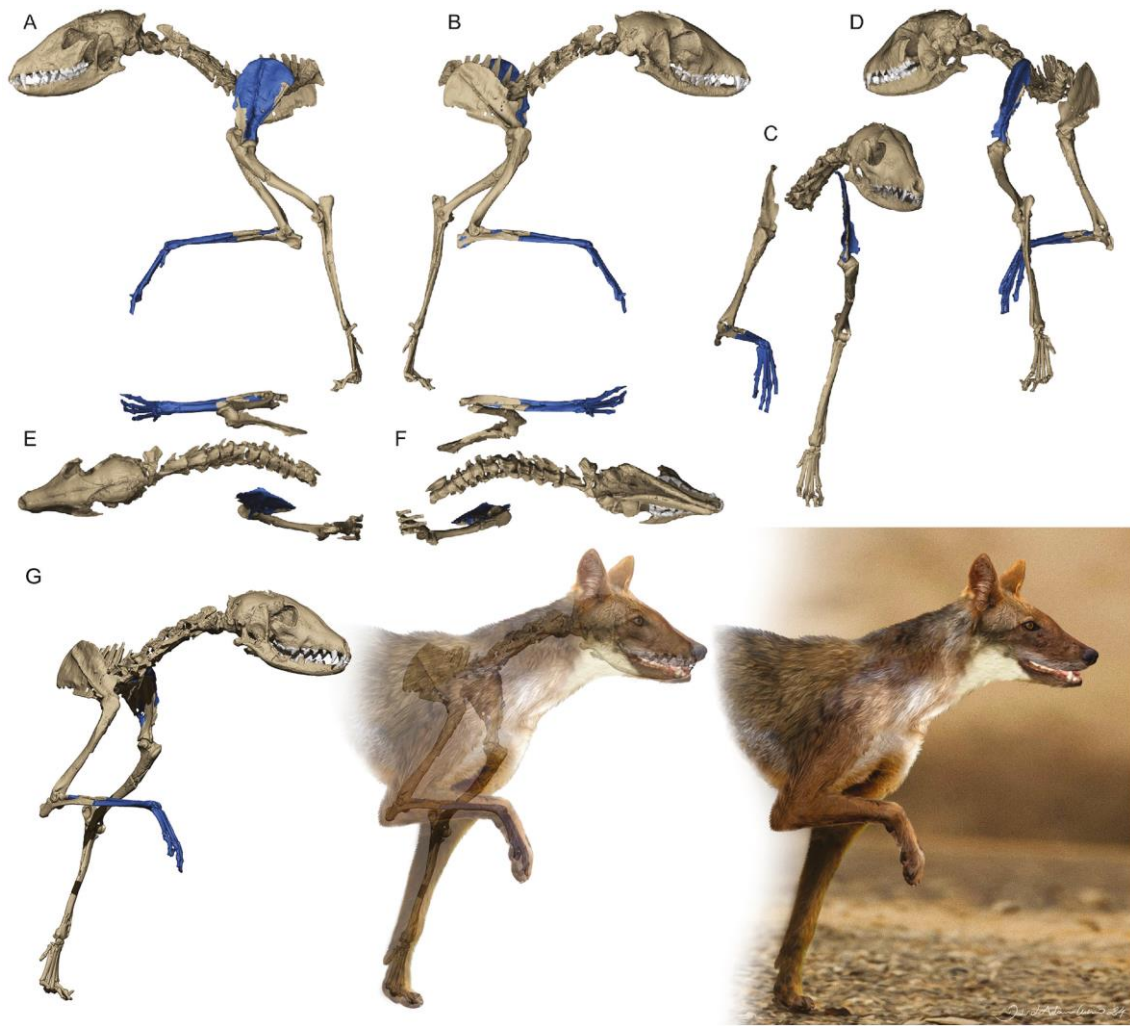


**Table 1.** Measurements (mm) of the cranium and upper teeth of MGPT-PU 135418 from Verduno (Italy). Values in brackets were estimated.

<i>Cranium</i>		<i>Upper teeth</i>	Left	Right
Total length	180.0	I1 length	2.8	3.1
Condylobasal length	166.2	I1 breadth	2.5	2.8
Basal length	173.7	I2 length	3.3	3.8
Upper neurocranium length	89.7	I2 breadth	2.9	3.0
Splanchnocranium length	76.6	I3 length	4.2	4.1
Facial length	99.2	I3 breadth	3.2	3.3
Greatest length of the nasals	63.7	C length	7.6	7.3
Palatal length	87.6	C breadth	5.1	4.9
Length of the cheektooth row	63.5	P1 length	4.7	4.4
Length of the molar row	18.0	P1 breadth	3.1	3.0
Length of the premolar row	47.8	P2 length	9.0	8.2
Greatest diameter of the auditory bulla	24.5	P2 breadth	3.4	3.3
Greatest mastoid breadth	53.5	P3 length	9.5	10.2
Breadth dorsal to the external auditory meatus	55.1	P3 breadth	3.6	3.9
Greatest breadth of the occipital condyles	(30.5)	P4 length	15.1	15.9
Greatest breadth of the bases of the paraoccipital processes	42.1	P4 breadth	6.0	6.2
Greatest breadth of the foramen magnum	(14.2)	P4 max breadth	7.91	8.0
Height of the foramen magnum	(10.4)	P4 metastyle length	6.2	6.5

Greatest neurocranium breadth	55.6	M1 length	11.2	12.1
Zygomatic breadth	(77.0)	M1 breadth	13.5	13.9
Least breadth of cranium (at postorbital constriction)	32.7	M2 length	7.2	7.2
Frontal breadth	(47.0)	M2 breadth	9.9	9.6
Least breadth between the orbits	36.7			
Greatest palatal breadth	51.3			
Least palatal breadth	26.5			
Breadth at the canine alveoli	27.2			
Greatest inner height of the orbit	27.0			
Height of the occipital triangle	(38.1)			

**Table 2.** Measurements (mm) of the mandible and lower teeth of MGPT-PU 135418 from Verduno (Italy). Values in brackets were estimated. Abbreviation: alv, measurement taken at the alveolus.

<i>Mandible</i>		<i>Lower teeth</i>	Left	Right
Total length: condyle process - Infradentale	133.1	i1 length	-	-
Length: angular process - Infradentale	133.3	i1 breadth	-	-
Length: indentation between the condyle process and the angular process - Infradentale	126.9	i2 length	2.1	2.3
Length: condyle process - distal border of canine alveolus	126.0	i2 breadth	2.4	2.4
Length: condyle process - mesial border of canine alveolus	130.3	i3 length	3.1	3.0
Length: indentation between the condyle process and the angular process - distal border of canine alveolus	119.3	i3 breadth	2.7	2.8

Length: angular process - distal border of canine alveolus	125.6	c length	7.4	7.5
Length: distal border of m3 alveolus - distal border of canine alveolus	83.0	c breadth	5.1	5.2
Length of the cheektooth row p1-m3	71.7	p1 length	4.1	3.9 alv.
Length of the cheektooth row p2-m3	63.4	p1 breadth	2.4	2.7 alv.
Length of the molar row m1-m3	(32.9)	p2 length	7.6	7.5
Length of the premolar row p1-p4	40.2	p2 breadth	3.2	3.6
Length of the premolar row p2-p4	31.4	p3 length	8.8	9.0
Greatest thickness of mandibular corpus	10.3	p3 breadth	3.3	3.6
Height of the ramus: basal point of the angular process - Coronion	57.4	p4 length	10.3	10.2
Height basal point of the angular process - condyle process	26.3	p4 breadth	4.0	3.9
Height of the mandible behind m1	24.1	m1 max length	17.1	17.2
Height of the mandible between p2 and p3	15.6	m1 breadth	7.3	7.1
Height of the mandible behind canine	11.4	m1 blade length	11.6	11.9
		m2 length	8.9	9.0
		m2 breadth	6.2	6.4
		m3 length	(4.8)	5.4
		m3 breadth	3.0	4.6

**Table 3.** Measurements (mm) of the postcranial bones of MGPT-PU 135418 from Verduno (Italy). Values in brackets were estimated.

Greatest length (GL)	28.7	
Greatest breadth (over the wings) (GB)	(66.0)	
Length of the dorsal arch	(11.0)	
Greatest breadth of the cranial articular surface (BFcr)	31.7	
Greatest breadth of the caudal articular surface (BFcd)	24.4	
Height (H)	25.3	
Greatest length from cranial to caudal articular surfaces (GLF)	22.4	
<i>Axis</i>		
Greatest length of the body (LCDe)	43.0	
Smallest breadth	18.2	
Greatest breadth across <i>Processus articulares caudales</i>	25.5	
Greatest breadth of the cranial articular surface (BFcr)	21.8	
Height (H)	(30.0)	
Height of the spinous process (HSp)	13.1	
<i>Scapula</i>	Left	Right
Height along the spine	-	110.8
Length of glenoid cavity	18.6	19.7
Smallest length of the scapular neck	(20.0 )	22.0
Greatest length of the <i>Processus articularis</i> (GLP)	21.6	22.7
Breadth of the glenoid cavity	12.0	(13.0)

<i>Humerus</i>	Left	Right
Greatest length (GL)	141. 6	145.4
Greatest length from the head (GLC)	139. 4	142.2
Greatest height of the head (GHC)	13.1	13.4
Depth of proximal end (Dp)	31.8	33.4
Smallest breadth of diaphysis (SDcr) in cranial view	9.1	9.1
Greatest breadth of distal end (Bd)	24.2	24.5
Greatest breadth of the trochlea (BT)	18.6	17.6
Greatest height of the trochlea (Ht)	13.1	13.1
Height of the medial epicondyle (Hme)	6.1	6.1
Breadth of the lateral epicondyle (Ble)	16.1	16.3
<i>Radius</i>	Left	Right
Greatest length (GL)	132. 3	-
Greatest breadth of proximal end (Bp)	13.5	13.5
Greatest depth of proximal end (Dp)	8.9	8.7
Smallest breadth of diaphysis (SDcr) in cranial view	10.0	-
Smallest breadth of diaphysis (SDl) in lateral view	6.2	-
Greatest breadth of distal end (Bd)	18.2	-
Greatest depth of distal end (Dd)	10.1	-
<i>Ulna</i>	Left	Right

Greatest length (GL)	155.8	-			
Depth across the Processus anconaeus (DPA)	19.2	19.5			
Smallest depth of the olecranon (SDO)	17.4	16.9			
Smallest breadth of the olecranon (SBO)	8.1	7.7			
Greatest breadth across the coronoid process (BPC)	11.2	11.5			
Length: top of the olecranon - coronoid process	28.3	(28.7)			
Length: anconeal process - coronoid process	13.9	(13.7)			
Length: top of the olecranon - anconeal process	14.6	(14.7)			
Smallest breadth of diaphysis (SDcr) in cranial view	6.7	-			
Smallest breadth of diaphysis (SDl) in lateral view	12.0	-			
<i>Metacarpals</i>	I	II	III	IV	V
Greatest length (GL)	17.1	46.3	54.0	54.0	45.9
Greatest breadth of the proximal end (Bp)	-	5.9	5.9	5.6	8.3
Greatest depth of the proximal end (Dp)	5.6	7.9	8.0	7.4	7.6
Smallest breadth of the diaphysis (SD)	3.2	5.1	5.2	4.5	6.0
Greatest breadth of the distal end (Bd)	4.8	7.5	6.4	7.0	8.9
Greatest depth of the distal end (Dd)	4.5	5.0	5.9	6.9	6.4
<i>Digit I</i>	Phalanx I	Phalanx II	Phalanx III		
Greatest length (GL)	9.3	-	-		
Greatest breadth of the proximal end (Bp)	5.4	-	-		
Greatest depth of the proximal end (Dp)	4.3	-	-		

Smallest breadth of the diaphysis (SD)	4.2	-	-
Greatest breadth of the distal end (Bd)	4.5	-	-
Greatest depth of the distal end (Dd)	3.2	-	-
<i>Digit II</i>	Phal anx I	Phalanx II	Phalanx III
Greatest length (GL)	17.5	11.0	-
Greatest breadth of the proximal end (Bp)	6.9	6.1	-
Greatest depth of the proximal end (Dp)	6.5	5.7	-
Smallest breadth of the diaphysis (SD)	4.7	4.7	-
Greatest breadth of the distal end (Bd)	5.4	5.6	-
Greatest depth of the distal end (Dd)	4.5	4.2	-
<i>Digit III</i>	Phal anx I	Phalanx II	Phalanx III
Greatest length (GL)	20.6	14.6	12.2
Greatest breadth of the proximal end (Bp)	6.7	6.1	5.4
Greatest depth of the proximal end (Dp)	5.9	5.4	8.2
Smallest breadth of the diaphysis (SD)	4.2	4.2	-
Greatest breadth of the distal end (Bd)	5.3	5.4	-
Greatest depth of the distal end (Dd)	4.3	4.1	-
<i>Digit IV</i>	Phal anx I	Phalanx II	Phalanx III
Greatest length (GL)	20.6	14.3	11.2
Greatest breadth of the proximal end (Bp)	6.8	6.0	5.1
Greatest depth of the proximal end (Dp)	5.7	5.1	8.0

Smallest breadth of the diaphysis (SD)	4.6	4.3	-
Greatest breadth of the distal end (Bd)	5.4	5.4	-
Greatest depth of the distal end (Dd)	4.3	4.2	-
<i>Digit V</i>	Phal anx I	Phalanx II	Phalanx III
Greatest length (GL)	17.2	10.7	12.8
Greatest breadth of the proximal end (Bp)	7.4	6.5	5.1
Greatest depth of the proximal end (Dp)	6.2	5.7	8.3
Smallest breadth of the diaphysis (SD)	4.4	4.8	-
Greatest breadth of the distal end (Bd)	5.4	5.5	-
Greatest depth of the distal end (Dd)	4.3	-	-

**Table 4.** Estimations of the body mass based on average m1 length (m1L) in MGPT-PU 135418 and numerous *Eucyon* species. Abbreviation: N, sample size).

Species	N	m1L (mm)	Body mass (kg)
MGPT-PU 135418	1	17.18	11
<i>E. davisi</i> from Asia	4	17.53	11
<i>E. davisi</i> from North America	97	17.09	11
<i>E. ferox</i>	9	20.52	15
<i>E. zhoui</i>	3	17.73	11
<i>E. minor</i>	3	18.50	12
<i>E. marinae</i>	1	19.25	13
<i>E. cipio</i>	1	20.85	15
<i>E. monticinensis</i>	3	17.87	11

<i>E. debonisi</i>	13	16.04	9
<i>E. odessanus</i>	13	17.74	11
<i>E. adoxus</i>	3	18.02	12
<i>E. kuta</i>	1	17.00	10
<i>E. khoikhoi</i>	4	14.77	8

